An activated form of ADAM10 is tumor selective and regulates cancer stem-like cells and tumor growth

Lakmali Atapattu,[1]* Nayanendu Saha,[3]* Chanly Chheang,[1] Moritz F. Eissman,[4] Kai Xu,[3] Mary E. Vail,[1] Linda Hii,[1] Carmen Llerena,[1] Zhanqi Liu,[5] Katja Horvay,[2] Helen E. Abud,[2] Ulrike Kusebauch,[6] Robert L. Moritz,[6] Bi-Sen Ding,[7] Zhongwei Cao,[7] Shahin Rafii,[7] Matthias Ernst,[4] Andrew M. Scott,[5] Dimitar B. Nikolov,[3] Martin Lackmann,[1] and Peter W. Janes[1]

[1]Cancer Program, Monash Biomedicine Discovery Institute and Department of Biochemistry and Molecular Biology and [2]Department of Anatomy and Developmental Biology, Monash University, Clayton, Victoria 3800, Australia
[3]Structural Biology Program, Memorial Sloan-Kettering Cancer Center, New York, NY 10065
[4]Cancer and Inflammation Laboratory and [5]Tumor Targeting Laboratory, Olivia Newton-John Cancer Research Institute and School of Cancer Medicine, La Trobe University, Heidelberg, Victoria 3084, Australia
[6]Institute for Systems Biology, Seattle, WA 98109
[7]Department of Genetic Medicine, Weill Cornell Medical College, New York, NY 10065

The transmembrane metalloprotease ADAM10 sheds a range of cell surface proteins, including ligands and receptors of the Notch, Eph, and erbB families, thereby activating signaling pathways critical for tumor initiation and maintenance. ADAM10 is thus a promising therapeutic target. Although widely expressed, its activity is normally tightly regulated. We now report prevalence of an active form of ADAM10 in tumors compared with normal tissues, in mouse models and humans, identified by our conformation-specific antibody mAb 8C7. Structure/function experiments indicate mAb 8C7 binds an active conformation dependent on disulfide isomerization and oxidative conditions, common in tumors. Moreover, this active ADAM10 form marks cancer stem-like cells with active Notch signaling, known to mediate chemoresistance. Importantly, specific targeting of active ADAM10 with 8C7 inhibits Notch activity and tumor growth in mouse models, particularly regrowth after chemotherapy. Our results indicate targeted inhibition of active ADAM10 as a potential therapy for ADAM10-dependent tumor development and drug resistance.

INTRODUCTION

ADAM (a disintegrin and metalloprotease) transmembrane metalloproteases (MPs) catalyze the release of a range of cell surface proteins, activating receptor tyrosine kinase (RTK), Notch, cytokine, chemokine, and adhesion signaling pathways important in normal and oncogenic development. Prominent oncogenic substrates include ligands and receptors in the Notch, erbB, and Eph families, cytokines (TNF and IL6), FAS ligand, Slit, L-selectin, and cadherins (Murphy, 2008), which are all shed by one of two closely related and widely expressed proteases, ADAM10 and ADAM17 (or TACE [TNF converting enzyme]). These proteases are also frequently overexpressed in cancers, correlating with aberrant signaling and poor patient prognosis, including cancers of the colon, lung, stomach, uterus, and ovary (Pruessmeyer and Ludwig, 2009). They are thus potent activators of key oncogenic pathways and recognized targets for multipathway inhibition (Murphy, 2008; Hartmann et al., 2013).

ADAM10 in particular acts as principal sheddase for Notch (Hartmann et al., 2002), Eph (Hattori et al., 2000; Janes et al., 2005), and certain epidermal growth factor receptor (EGFR) ligands (Sahin et al., 2004), as well as E- and N-cadherin (Reiss et al., 2005). The resemblance of ADAM10 and Notch-deficient mice, including embryonic defects in somitogenesis, neurogenesis, and vasculogenesis (Hartmann et al., 2002; Saftig and Reiss, 2011), highlights a critical role for ADAM10 in canonical ligand-activated Notch signaling in particular. Notch signaling is triggered by binding of cell surface–bound ligands, Delta-Like (1–4) or Jagged (1 and 2), to Notch receptors (Notch1–4), which initiates ADAM-mediated shedding of both ligand (LaVoie and Selkoe, 2003) and receptor extracellular domains (ECDs; Kopan and Ilagan,

Dr. Lackmann died on 22 May 2014.

*L. Atapattu and N. Saha contributed equally to this paper.

Correspondence to Peter W. Janes: peter.janes@monash.edu

L. Atapattu's present address is Children's Cancer Institute, Lowy Cancer Research Centre, University of New South Wales, Randwick, New South Wales 2031, Australia.

Abbreviations used: ADAM, a disintegrin and metalloprotease; CDR, complementarity determining region; CRC, colorectal cancer; CSC, cancer stem cell; ECD, extracellular domain; EGFR, epidermal growth factor receptor; EMT, epithelial to mesenchymal transition; GSI, γ-secretase inhibitor; HMW, high molecular weight; IF, immunofluorescence; IHC, immunohistochemistry; IP, immunoprecipitation; LMW, low molecular weight; MMP, matrix MP; MP, metalloprotease; MPB, maleimide-PEG2-biotin; NICD, notch intracellular domain; PDI, protein disulfide isomerase; ROS, reactive oxygen species; RTK, receptor tyrosine kinase; WB, Western blot.

The Rockefeller University Press $30.00
J. Exp. Med. 2016 Vol. 213 No. 9 1741–1757
www.jem.org/cgi/doi/10.1084/jem.20151095

2009). Shedding of the notch ECD provides the signal for γ-secretases to cleave and release the Notch intracellular domain (NICD), acting as transcriptional activator for an extensive set of genes, regulating cell proliferation, differentiation, epithelial to mesenchymal transition (EMT), and cell survival (Kopan and Ilagan, 2009). Deregulated Notch signaling promotes the progression of solid cancers (Ranganathan et al., 2011) by driving angiogenesis (Roca and Adams, 2007) and maintaining undifferentiated, cancer stem cells (CSCs), thought to initiate and sustain tumor growth and promote metastasis and chemoresistance (Espinoza et al., 2013; Giancotti, 2013). However, pan-specific γ-secretase inhibitors (GSIs) blocking NICD release (Groth and Fortini, 2012) cause severe intestinal toxicity, likely reflecting the diversity of γ-secretase targets (Dikic and Schmidt, 2010). Similarly, small-molecule inhibitors blocking the ADAM protease active site failed clinical development, initially because of, at least in part, off-target effects, reflecting the close structural similarity of this site in all matrix MPs (MMPs; DasGupta et al., 2009; Saftig and Reiss, 2011). In support, more specific ADAM inhibitors, with limited MMP targets, show no adverse effects associated with MMP inhibition, such as fibroplasias (Fridman et al., 2007).

The ADAM ECD contains an N-terminal pro-sequence followed by MP (M), disintegrin (D), cysteine-rich (C), transmembrane, and cytoplasmic domains (Hartmann et al., 2013). Proteolytic specificity is not simply caused by a typical substrate cleavage signature, but relies on noncatalytic interactions of the substrate with the ADAM C domain to position the substrate for effective cleavage (Smith et al., 2002; Janes et al., 2005, 2009). In addition, emerging evidence suggests that ADAM17 is regulated by adopting latent and active ECD conformations, dependent on redox state, because mild reducing or oxidizing conditions alter ADAM17 activity, as well as its recognition by conformation-specific antibodies (Wang et al., 2009; Willems et al., 2010). This is proposed to depend on disulfide bond isomerization involving a thioredoxin CxxC motif in the ADAM17 C domain, a motif targeted for disulfide exchange catalyzed by protein disulfide isomerases (PDIs; Benham, 2012), and indeed PDI treatment does alter ADAM17 activity (Willems et al., 2010). ADAM10 also contains this conserved motif, suggesting it may be similarly regulated by redox conditions. Considering that reactive oxygen species (ROS), frequently elevated in tumors because of RTK and proinflammatory signaling, are known to activate ADAM10/17 (Wang et al., 1996; Fischer et al., 2004), this effect on ECD conformation may help explain how kinase-dependent cytosolic signaling regulates the activity of the extracellular ADAM protease domain (Hattori et al., 2000; López-Otín and Hunter, 2010; Hartmann et al., 2013; Atapattu et al., 2014).

We previously determined the structure of the ADAM10 D+C domains and identified a substrate-binding pocket within the C domain that specifies ligand cleavage (Janes et al., 2005). We also raised antibodies against ADAM10, one of which, mAb 8C7, specifically recognized the substrate-binding C domain and inhibited ADAM10-mediated cleavage of Eph receptor ligands (ephrins) and ephrin/Eph-dependent signaling and cell segregation in vitro (Atapattu et al., 2012). We thus sought to test the mechanism of action of 8C7 and its efficacy for tumor growth inhibition. We find 8C7 specifically binds a CxxC-dependent, active form of ADAM10, which we detect preferentially in tumors compared with normal tissues. Moreover, the 8C7-recognized, active ADAM10 particularly marks CSC-like cells with high Notch activity, and 8C7 treatment inhibits Notch signaling and tumor growth in mouse models, particularly regrowth after chemotherapy.

RESULTS

Preferential targeting of ADAM10 in tumors

We tested our anti-ADAM10 mAb 8C7 in a LIM1215 colorectal cancer (CRC) xenograft model, which displays high levels of ADAM10, Notch, Eph, and erbB receptors. We first analyzed targeting to tumors and other tissues of tumor-bearing mice by injection of Alexa-labeled 8C7 and subsequent analysis of tumor and organ tissues by immunofluorescence (IF) microscopy. Remarkably, despite 8C7 recognizing both mouse and human ADAM10 (Atapattu et al., 2012), it selectively bound to tumors, particularly to cells near vessels (marked with rhodamine-lectin) and near the tumor rim, with only slight or undetectable binding to other organs (Fig. 1, A and B). In comparison, a commercial ADAM10 antibody (MAB946) recognizing both human and mouse ADAM10 strongly stained multiple tissues (Fig. 1 B, last column), consistent with the ubiquitous expression of ADAM10. We also recovered 8C7-bound ADAM10 from tumors and organs of mice injected with 8C7, or PBS as control, by incubating protein extracts with protein A Sepharose. ADAM10 was clearly detected in protein A pull-downs from tumors (Fig. 1 C, top), with much lower or undetectable binding in tissues. In comparison, immunoprecipitation (IP) with control ADAM10 mAb showed ADAM10 was widely present (Fig. 1 C, bottom). Interestingly, in normal tissues, ADAM10 was predominately detected as a low molecular weight (LMW; processed) form, whereas tumors also prominently expressed a high molecular weight (HMW; unprocessed) form, which was also clearly targeted by 8C7.

Identification of a distinct, 8C7-recognized, active form of ADAM10 in tumor cells

To test whether this 8C7-recognized, HMW form of ADAM10 is found in human tumors, we conducted IP experiments with normal and human tumor tissues using 8C7 or another anti-ADAM10 mAb we raised (4A11), following the approach outlined previously (Atapattu et al., 2012), as control. Unlike 8C7, which binds both human and mouse ADAM10, 4A11 recognizes only human ADAM10 (Fig. 2 A). Analysis of colon tumors and matched normal tissues showed marked presence of HMW ADAM10 in tumors, with very little or undetectable amounts in normal tissues (Fig. 2 B).

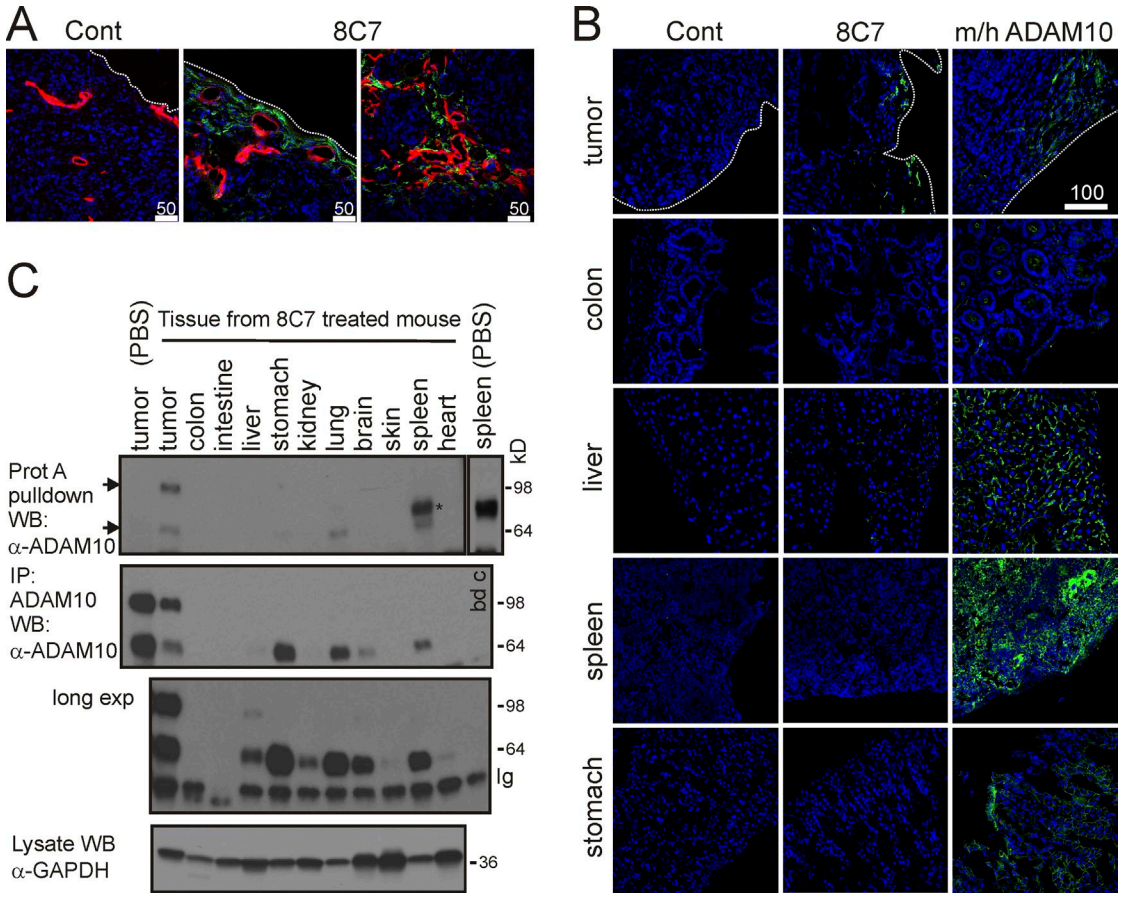

Figure 1. **Anti-ADAM10 mAb 8C7 preferentially binds ADAM10 in tumors.** (A) Immunofluorescent confocal microscopy of LIM1215 xenograft tumor sections from mice preinjected with Alexa-labeled 8C7 or IgG control (100 µg, 48 h prior) and rhodamine-lectin (15 min prior). 8C7 binding (green) is strongest near blood vessels (labeled by rhodamine lectin, red) and the tumor rim (marked by dotted lines). Hoechst stain shows nuclei (blue). (B) Fluorescence microscopy of tumor and tissue sections from mice preinjected 48 h prior with 100 µg Alexa-labeled 8C7 or control ADAM10 antibody MAB946 (both antibodies recognize human and mouse ADAM10) or IgG control. (A and B) Scale bars are in micrometers. (C) WB analysis of 8C7-bound ADAM10 recovered by protein A Sepharose from tissue lysates of tumor-bearing mice, injected with 1 mg 8C7 or PBS (top). Bottom panels show overall ADAM10 expression by IP/WB with a control antibody recognizing mouse and human ADAM10 (Abcam pAb 39177) and lysate loading control (GAPDH). HMW ADAM10 is prevalent in tumors. The asterisk indicates a nonspecific band from spleen in both 8C7- and PBS-injected mice. bd c, 8C7-bead–only control. Panels show data representative of three independent experiments.

Interestingly, the HMW form was preferentially recognized by 8C7 compared with 4A11, and although 8C7 can also bind the LMW form, it consistently binds more to the HMW form in tumor cell lysates relative to 4A11 or other control ADAM10 antibodies (see also Fig. 4).

The aforementioned data suggest 8C7 preferentially targets an unprocessed form of ADAM10 predominantly found in tumors. Full-length, unprocessed ADAM10 contains a prodomain that is released by furin or other pro-protein convertases to produce the processed mature form. We confirmed the HMW form is present on the cell surface (Fig. 2 C) and is indeed nonprocessed, as it could be converted to LMW ADAM10 by incubation with furin (Fig. 2 D), and mass spectrometry analysis of HMW and LMW bands from ADAM10 IPs resolved by SDS-PAGE detected Pro domain peptides only in the HMW band (not depicted). Processing has been suggested to produce the active form of ADAMs by releasing the Pro domain, which can interact with and inhibit the mature MP, although for ADAM10 and 17 this does not occur via the cysteine switch mechanism of other MPs (Moss et al., 2007). However, the Pro domain has also been shown to have a necessary chaperone function, and recombinant Pro domain rescues activity of an inactive, prodomain-deleted form of ADAM10 (Anders et al., 2001). We therefore tested whether 8C7-targeted ADAM10 represents an active or inactive population. 8C7 and 4A11 IPs from LIM1215 cell lysates were first adjusted to contain similar amounts of ADAM10 (confirmed by Western blot [WB]; Fig. 2 E, left panels), and parallel samples were then incubated with a quenched fluorogenic peptide substrate that fluoresces only when cleaved (Es003; R&D Systems). 8C7-bound ADAM10 showed much higher activity compared with control 4A11 IPs, relative to ADAM10

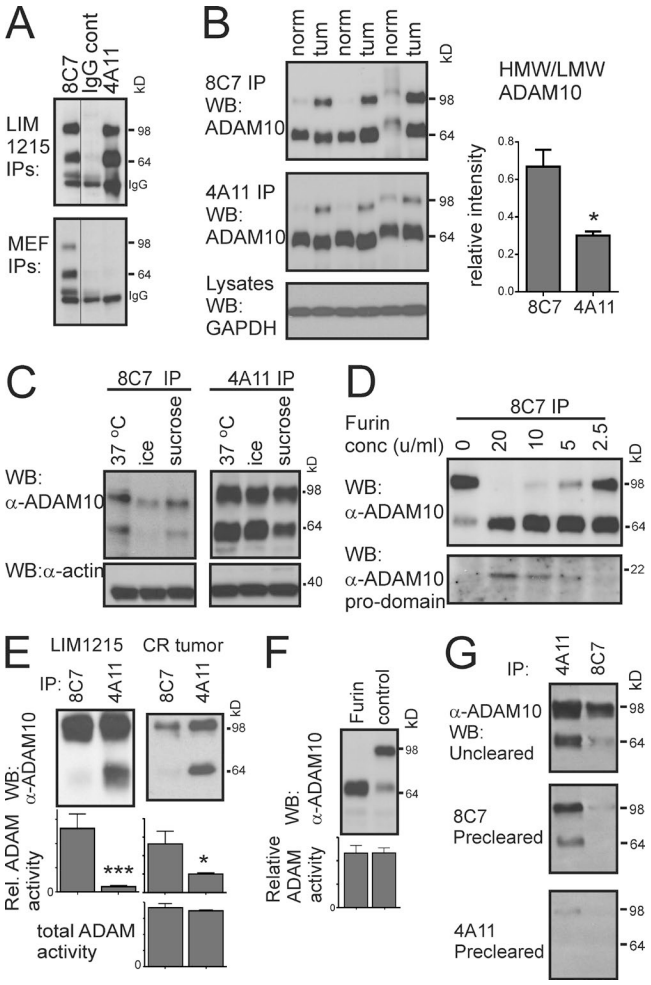

Figure 2. **mAb 8C7 preferentially binds an active form of ADAM10 in tumors.** (A) Immunoprecipitates with anti-ADAM10 mAbs 8C7 and 4A11, or an isotype-matched IgG control, from lysates of LIM1215 human tumor cells or mouse embryonic fibroblasts (MEFs; irrelevant lane removed, as indicated by black lines). (B) Immunoprecipitates of ADAM10 from human colorectal tumors (tum) or matched normal (norm) tissue samples with 8C7 or control ADAM10 mAb 4A11, Western blotted for ADAM10 (top panel represents longer exposure time). Total lysates were blotted for GAPDH as loading control. Graph shows relative levels of HMW and LMW ADAM10 bands in each sample (mean ± SEM; $n = 3$; *, $P < 0.05$ by unpaired two-tailed Student's t test). (C) The HMW form of ADAM10 is present on the cell surface. Intact LIM1215 cells were incubated with 8C7 or 4A11 at 37°C or under conditions inhibiting endocytosis (on ice or in the presence of 0.4 M sucrose). Cells were washed and lysed, and protein A beads were added to pull down mAb-bound ADAM10. Samples were analyzed by WB with α-ADAM10 pAb. (D) Furin treatment confirms HMW ADAM10 is unprocessed. 8C7 and 4A11 IPs from LIM1215 lysates were treated with a dose range of recombinant Furin for 1 h, and samples were analyzed by WB with an α-ADAM10 pAb and an ADAM10 pro-domain–specific antibody. (E) Activity assays and matching WBs of nonreduced ADAM10 immunoprecipitates from lysates of LIM1215 cells (left) or human CRC tumor tissue (right), using a quenched fluorescent peptide substrate that fluoresces upon cleavage (FRET assay; mean ± SEM; $n = 3$ experiments; *, $P = 0.05$; ***, $P < 0.001$ by unpaired two-tailed Student's t test). In the left panel, immunoprecipitates were adjusted to have similar levels of ADAM10, and activity is expressed relative to ADAM10 levels (bottom panel, arbitrary units). For the tumor samples (right), IPs were from lysates with equal total protein, and both relative and total activity are shown. (F) Processing does not alter ADAM10 activity. 8C7 IPs from whole cell LIM1215 lysates were treated with recombinant Furin (20 U/ml, 1 h) or left untreated before assay for ADAM10 sheddase activity using a quenched fluorogenic peptide substrate. Activity was determined relative to ADAM10 levels as in E (mean ± SEM; $n = 3$). (G) Sequential IP of LIM1215 cell lysates with 4A11 and 8C7. Top panel shows WB of ADAM10 recovered from initial precipitations; bottom panels show subsequent precipitations from remaining precleared supernatants as indicated. All data are representative of at least two independent experiments.

levels (Fig. 2 E, left). Similar results were obtained from human colorectal tumor tissue, where 8C7 IPs from lysates (with equal total protein content) had higher activity relative to ADAM10 levels, while overall activity of 8C7 and 4A11 IPs was equal (Fig. 2 E, right). This shows that 8C7-bound ADAM10 retains activity in its MP domain (i.e., it is able to cleave a peptide in solution), consistent with binding of 8C7 to the noncatalytic C domain, and indicates its preferential binding to a conformation with high activity. In these experiments, 8C7 led to predominant pull-down of unprocessed ADAM10, indicating processing is not required for activity, as recently reported also for ADAM17 (Le Gall et al., 2010), and indeed treatment of ADAM10 immunoprecipitates with furin had no effect on activity (Fig. 2 F). Lastly, sequential IP experiments confirmed that 8C7 only binds a subset of ADAM10 because LIM1215 lysate precleared with 8C7 still retained ADAM10 recovered by 4A11 (but not 8C7), whereas 4A11 precleared lysate did not (Fig. 2 G). Thus, our data show a subpopulation of ADAM10 on tumor cells with high protease activity that is preferentially recognized by mAb 8C7 and that does not require processing, but rather is prominent in a nonprocessed ADAM10 population.

Structure of the ADAM10 D+C/8C7 complex and dependence of 8C7 binding on CxxC motif modulation

We then set out to investigate the determinants of 8C7 specificity for active ADAM10. We have previously shown that 8C7 binds the cysteine-rich (C) domain of ADAM10 (Atapattu et al., 2012), and we have also previously determined the structure of this domain along with the adjacent disintegrin (D) domain, revealing a continuous, elongated, slightly curved structure with a negatively charged pocket mediating ADAM10-substrate recognition (Janes et al., 2005). To define the exact binding site of 8C7, we determined the structure of ADAM10 D+C domains in complex with the isolated $F(ab')_2$ fragment of 8C7 at 2.76-Å resolution (Fig. 3). The 8C7-bound ADAM10 D+C structure is very similar to that of the unbound ADAM10 D+C (Janes et al., 2005), and they can be superimposed with a root-mean-square deviation (r.m.s.d.) of 1.28 Å between 133 Cα atoms. However, in the mAb-bound ADAM10 structure an additional N-terminal segment in the disintegrin domain (residues 450–482) is detectable,

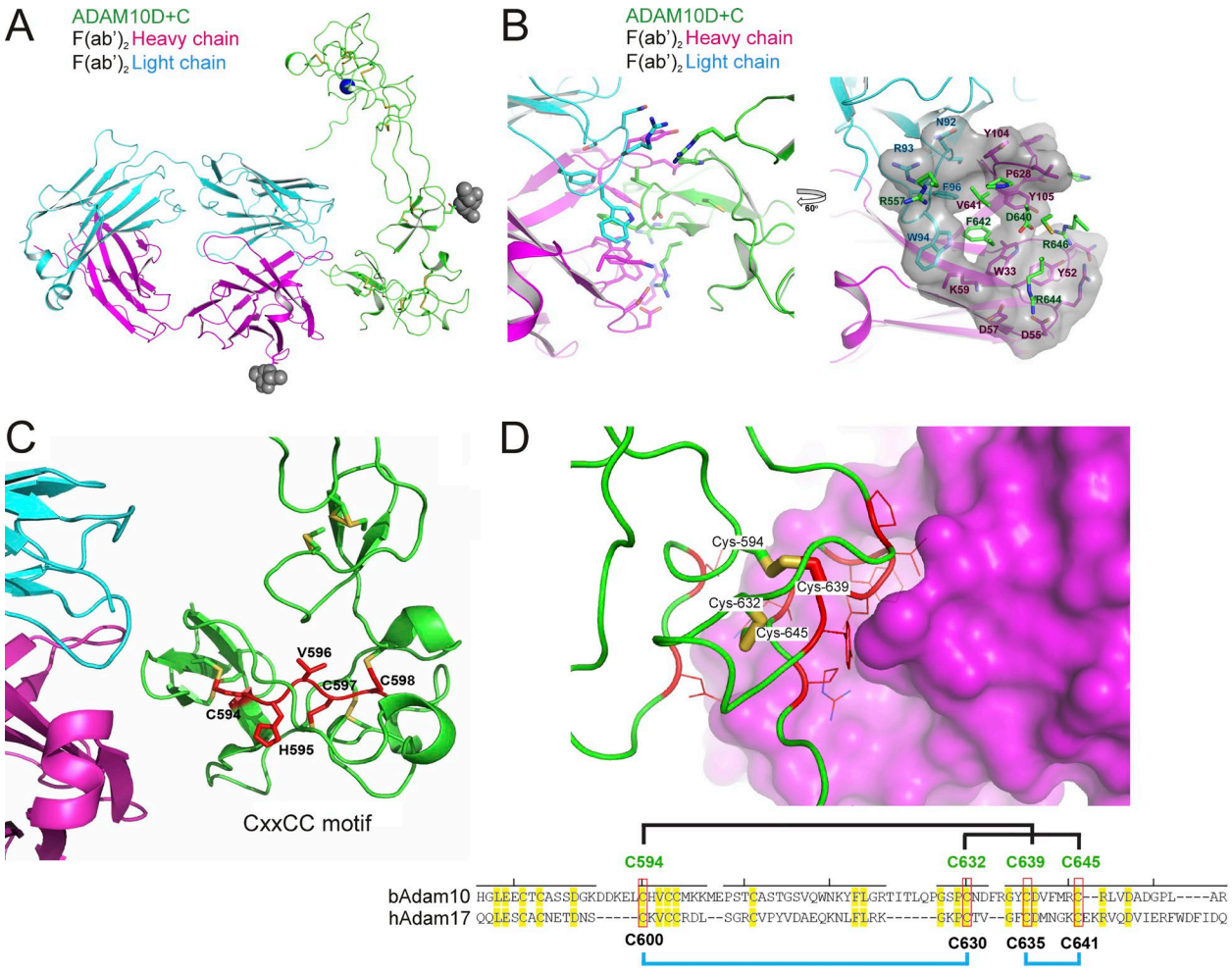

Figure 3. **Crystal structure of the 8C7 F(ab′)$_2$/ADAM10 D+C complex.** (A) The heavy chain of the 8C7 mAb is in magenta, and the light chain is in cyan. The disintegrin and cysteine-rich domains of ADAM10 are in green. Disulfide bridges in ADAM10 are drawn as sticks and colored in yellow. Glycosylation moieties are drawn as gray spheres. A calcium ion, bound in the ADAM disintegrin domain, is in blue. There are two copies of the ADAM10 D+C/8C7 F(ab′)$_2$ fragment complex in the asymmetric unit, which are nearly identical with an r.m.s.d. of 0.62 Å for 557 Cα atoms. (B) Two close-up views of the 8C7/ADAM10 interface. The right panel view is a 60-degree rotation from the left panel view. The heavy chain of the 8C7 mAb is in magenta, the light is in cyan, and ADAM10 is in green. The interacting residues are drawn as sticks and labeled on the right panel. The molecular surface of 8C7, which is in contact with ADAM10, is rendered in gray on the right panel. (C) The ADAM10/Mab complex structure highlighting the position of the bound 8C7 relative to the location of the CxxC motif. (D) Close up of the 8C7/ADAM10 interface showing interacting residues (red) in ADAM10, including C639, which forms a disulfide bond (yellow) with C594 of the CxxC motif. A space-filled representation of the 8C7 F(ab′)$_2$ is shown (magenta). The sequence alignment at the bottom shows disulfide bonding observed in our ADAM10 structures (black lines) and an alternate disulfide pattern (blue lines) predicted from experiments on ADAM17 (Düsterhöft et al., 2013). Conserved residues are highlighted in yellow, with cysteines in red boxes.

as is a calcium-binding site in the disintegrin domain and an N-linked glycosylation site (N551) in the cysteine-rich domain (Fig. 3 A; additional supplementary information is shown in Table S1).

Formation of the F(ab′)$_2$/ADAM10 (D+C) complex buries ∼900 Å^2 of surface area in each molecule (Fig. 3 B). The antibody complementarity determining regions (CDRs) target the C domain of ADAM10 as expected, via residues on the third CDR of the light chain (CDR-L3) and heavy-chain CDR-H1-3. The center of this interface is formed by the insertion of two hydrophobic ADAM10 residues, V641 and F642, into a hydrophobic pocket defined by CDR-L3 residues (S_{91}, N_{92}, W_{94}, and F_{96}) and CDR-H1-3 residues (W_{33}, K_{59}, L_{103}, Y_{104}, and Y_{105}). Two adjacent ADAM10 residues (P_{628} and C_{639}) also contribute to the hydrophobicity of this central interface area by interacting with $Y104$ and L_{103} of the antibody CDR-H3. There are multiple hydrogen bonds in the surrounding regions that further stabilize the interaction, including hydrogen bonds between R_{644} (ADAM10) and D_{55} and D_{57} (CDR-H2); between D_{640} (ADAM10) and Y_{105} (CDR-H3); and between R_{646} (ADAM10) and N_{31}, Y_{52}, and Y_{105} (CDR-H1-3).

Importantly, the 8C7 epitope protrudes away from the C-terminal part of the ADAM10 cysteine-rich domain, which harbors the substrate-binding residues Glu_{573}, Glu_{578}, and Glu_{579} (Janes et al., 2005). The bound region is stabilized by two intramolecular disulfide bonds, C_{594}-C_{639} and C_{632}-C_{645}; in the former, C_{639}, part of the central interface with 8C7, is bonded with C_{594}, in the ADAM10 sequence $C_{594}HVCC_{598}$ (Fig. 3, C and D). Interestingly, this sequence represents a conserved thioredoxin CxxC motif, a consensus sequence for PDI-catalyzed disulfide exchange reactions. This motif is also found in the analogous position of ADAM17, where it has been shown to be necessary for the modulation of its protease activity by PDI (Willems et al., 2010) and by redox changes, where oxidizing conditions promote activity (Wang et al., 2009). This indicates disulfide isomerization underlies activity-related conformational changes, a notion supported by experiments showing PDI treatment alters recognition of ADAM17 by conformation-specific antibodies (Willems et al., 2010). Indeed, a recent nuclear magnetic resonance study revealed two distinct, PDI-regulated conformations of bacterially expressed ADAM17, with distinct disulfide bond arrangements of the CxxC residues (Düsterhöft et al., 2013). The analogous changes in ADAM10 would correspond to the C_{594}-C_{639} disulfide linkage in our 8C7-bound structure swapped to C_{594}-C_{632}, accompanied by a switch from C_{632}-C_{645} to C_{639}-C_{645}. Notably, these residues are all closely situated in the structure (Fig. 3 D).

We thus tested whether 8C7 binding was dependent on CxxC modulation. Mutation of the CxxC motif to AxxA clearly ablated binding of 8C7, but not of control antibodies (Fig. 4 A). Treatment of LIM1215 cells with the oxidant H_2O_2 significantly increased binding of 8C7 to ADAM10, compared with control ADAM10 mAb 4A11, while reducing conditions inhibited binding (Fig. 4 B). Similarly, EGF or Eph RTK stimulation, known to induce ROS (Chiarugi and Cirri, 2003), also increased binding of 8C7 to ADAM10, both in cell lysates (Fig. 4 B) and on intact cells (Fig. 4 C). Notably, 8C7-bound cells recovered from tumors showed markedly higher ROS levels compared with unbound cells (Fig. 4 D). Together, our observations show preferential binding of 8C7 to an active conformation of ADAM10 modulated by redox conditions and likely dependent on disulfide rearrangement. In support, treatment of ADAM10 IPs with recombinant PDI increased availability of free cysteines, as detected by labeling with the thiol-modifying reagent maleimide-PEG2-biotin (MPB; Fig. 4 E) and previously indicated by MS analysis of leukocytes (Metcalfe et al., 2011), indicating PDI-induced disulfide rearrangement of ADAM10. Furthermore, endogenous PDI was detected to coimmunoprecipitate with 8C7-bound ADAM10 by mass spectrometry (not depicted) and confirmed by WB analysis (Fig. 4 F).

8C7-recognized ADAM10 marks cancer stem–like cells containing active Notch signaling, which mAb 8C7 inhibits

Having ascertained that mAb 8C7 recognizes an active form of ADAM10, we wished to identify the subpopulation of tumor cells to which it most strongly binds (Fig. 1). ADAM10 plays an essential role in ligand-activated Notch signaling by releasing the ECD, and cells with active Notch have been identified in colon tumors, adjacent to vascular endothelial cells, where the endothelial cells supply the Notch ligand Jagged1 and the Notch active cells are marked by expression of the CSC marker CD133 (Lu et al., 2013). We therefore analyzed LIM1215 colon tumor xenografts from mice preinjected once with a low dose (100 µg) of $Alexa^{647}$-labeled 8C7, by costaining with antibodies against CD133 and against the NICD, which is generated by serial ADAM- and γ-secretase cleavage during active Notch signaling. We found that anti-CD133 clearly stained cells also targeted by 8C7 (Fig. 5 A). Similarly, antibodies against both NICD1 and NICD2 costained 8C7-targeted cells (82.7 ± 8.0% and 89.5 ± 4.5% of 8C7-bound cells costained for NICD1 and NICD2, respectively), indicating active Notch receptor signaling in these cells. Some costaining of $8C7^+$ cells with an antibody against human EpCam also suggests their epithelial tumor cell origin (Fig. 5 A), although the presence of $8C7^+$/$EpCam^-$ cells may also indicate EMT in this population. We confirmed Notch activity in the $CD133^+$ cells by FACS isolation of CD133-enriched and -depleted cell populations from tumors that, when compared for active NICD1 levels by WB, clearly showed high levels of Notch activity in the CD133-enriched population (Fig. 5 B). Lastly, antibodies against Jagged1 stained a distinct, lectin-labeled cell population, consistent with its reported endothelial expression in CRC (Fig. 5 C; Lu et al., 2013).

As we previously found mAb 8C7 inhibits ADAM10-mediated cleavage (Atapattu et al., 2012), we tested whether treatment (for 3 wk) with a higher dose (1 mg or 67 mg/kg) of 8C7 might inhibit Notch signaling in tumors by analyzing tumor lysates from control or 8C7-treated LIM1215 xenografts for active cleaved NICD1. 8C7 caused a significant inhibition of NICD levels compared with PBS-treated mice, whereas treatment with an isotype-matched control IgG did not inhibit (Fig. 6 A). Furthermore, expression of the Notch target Hes1 was also substantially decreased in tumors from 8C7- versus control IgG–treated mice (Fig. 6 B). We also confirmed inhibition of NICD levels in 8C7-treated tumors by immunohistochemistry (IHC; Fig. 6 C). Because ADAM10-mediated Notch signaling is important for continuous renewal of the intestinal mucosa (Tsai et al., 2014), we also investigated whether systemic 8C7 administration over three consecutive weeks would affect epithelial homeostasis in the proximal small intestine. In contrast to the profound effects on NICD staining in tumors, we did not detect significantly different patterns of NICD staining in intestinal crypts from control and 8C7-treated mice (Fig. 6 D). Likewise, we also observed similar staining patterns for the proliferation marker Ki67 and the intestinal stem cell marker Olfm4 (Fig. 6 D). Quantitative PCR analysis confirmed similar expression of Olfm4, Ki67, and Wnt-signaling target genes (Lgr5, Ascl-2, and c-myc), as well as markers for Paneth cells (Lzp) and secretory goblet cells (Muc-2) between control and 8C7-treated mice (Fig. 6 E). Collectively, our data suggest that

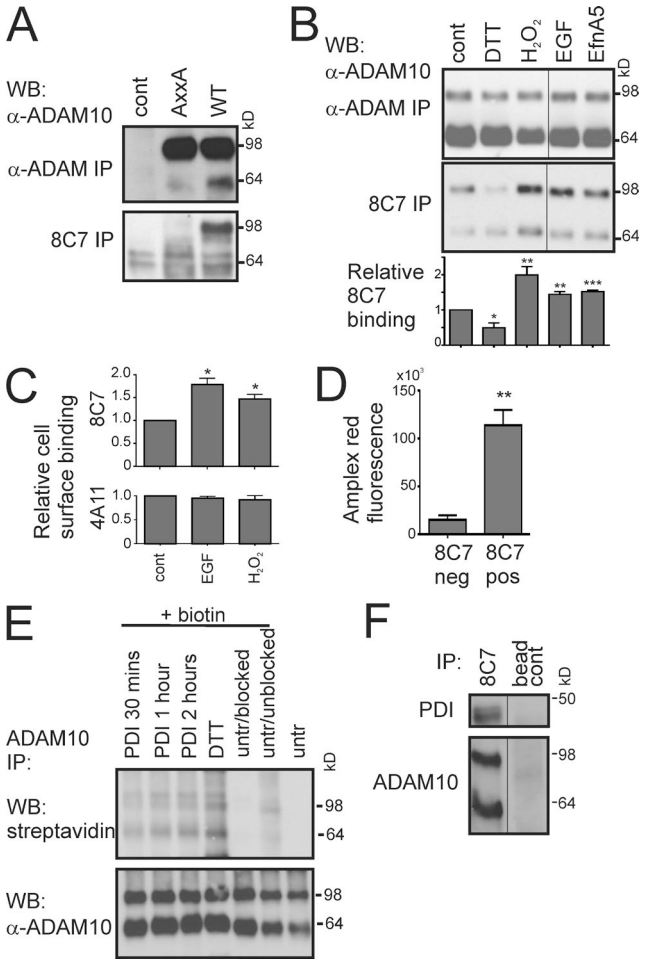

Figure 4. **8C7 binding to ADAM10 is dependent on the CxxC motif and redox conditions.** (A) Mutation of ADAM10 CxxC motif blocks binding of 8C7 but not control mAb. WT and AxxA mutant hADAM10 were transfected into ADAM10$^{-/-}$ mouse embryonic fibroblasts, and lysates were analyzed by IP with 8C7 and commercial (R&D Systems MAB1427) anti-ADAM10 antibodies and WB. (B) 8C7 binding to ADAM10 is modulated by redox conditions. LIM1215 cells were treated with reductant (DTT), oxidant (H_2O_2), or EGF or Eph RTK stimulation (with EGF or ephrin-A5 [EfnA5], respectively). ADAM10 was immunoprecipitated from cell lysates with 8C7 or control mAb 4A11 and analyzed by WB. Graph shows mean ± SEM; n = 6 experiments; *, $P < 0.05$; **, $P < 0.01$; ***, $P < 0.001$ by one-sample Student's t test relative to control. (C) Binding of Alexa-labeled 8C7 and 4A11 to cell surface ADAM10 on LIM1215 cells was assessed by flow cytometry in cells untreated or treated with 100 ng/ml EGF or 1 mM H_2O_2 for 30 min. Graphs show binding normalized to control cells; mean ± SEM; n = 3 experiments; *, $P < 0.05$ by one-sample Student's t test relative to control. (D) 8C7-targeted cells in tumors have high ROS production. Mice with LIM1215 xenografts were injected with 100 µg (6.7 mg/kg) Alexa^{647}-labeled 8C7, tumors were recovered, and 8C7-Alexa^{647}–positive and –negative cells were sorted by FACS. Equal cell numbers were then analyzed for ROS production by Amplex red assay. Graph shows mean ± SEM; n = 4 experiments; **, $P = 0.001$ by unpaired Student's t test. (E) PDI treatment exposes labile, disulfide-bonded cysteines. ADAM10 IPs from LIM1215 cell lysates were treated with methyl-PEG12-maleimide (MPM) to block free cysteines and then with PDI (5 µg/ml), or DTT (20 µM) as positive control, followed by MPB. Biotinylation and total ADAM10 levels were detected by WB using streptavidin-HRP and α-ADAM10 antibody, respectively. Untr, untreated with MPB. (F) PDI associates with 8C7-bound ADAM10 in cells. IPs from LIM1215 cell lysates with 8C7, 4A11, or control mAb were Western blotted with antibodies against PDI or ADAM10. (B and F) Black lines indicate that intervening lanes have been spliced out.

administration of 8C7 confers no detrimental effect on homeostatic renewal of the intestinal mucosa and on the stem cell and proliferative and differentiated epithelial cell compartments of the small intestine, consistent with our observation that extended treatment periods with 8C7 did not affect the body weight of mice (Figs. 7 C and 8 B). These observations support the aforementioned data indicating that 8C7 preferentially binds to ADAM10 in tumors.

To determine whether 8C7 can directly inhibit Notch signaling in vitro, we recovered tumor cells from LIM1215 xenografts and added HUVECs, expressing the Notch ligand Jagged1 (Cao et al., 2014). This stimulated Notch activity in the LIM1215 tumor cells, compared with either cell population alone, as determined by anti-NICD WB. Simultaneous treatment with 8C7, but not control IgG, inhibited this activation, as did GSI as positive control (Fig. 6 F). We also used a co-culture model in which Notch-dependent lymphoma survival and proliferation is afforded by contact with Jagged1-expressing HUVECs, which have been transduced with the adenoviral gene fragment E4ORF1 to drive Akt auto-activation and allow their serum-free propagation (Cao et al., 2014). Treatment with mAb 8C7 largely blocked lymphoma proliferation in this setting (Fig. 6 G), demonstrating effective inhibition of Notch.

Targeted inhibition of active ADAM10 inhibits tumor growth and relapse after chemotherapy

We then measured the effect of prolonged 8C7 treatment on tumor growth in the LIM1215 xenograft model. 8C7 treatment caused a significant, dose-dependent inhibition of tumor growth, as measured by tumor volume and weight (Fig. 7, A and B), but with no discernible detrimental effects on mouse health or weight (Fig. 7 C). In contrast, an isotype-matched control antibody did not inhibit tumor growth (Fig. 7 D). The treated tumors also displayed less vascular staining (α-CD31; Fig. 7 E) and increased apoptosis (TUNEL staining; Fig. 7 F), suggesting inhibitory effects on tumor angiogenesis, known to rely on Notch signaling, consistent with 8C7 inhibition of ADAM10-mediated Notch signaling in this context. Furthermore, after prolonged 8C7 treatment, there was decreased expression of ADAM10 and markedly less expression of Notch receptors, as well as Eph and MET receptors, which are coordinately expressed and associated with stem cell phenotype (Fig. 7 G; Finkbeiner et al., 2009; Gucciardo et al., 2014).

We also analyzed endogenously arising gastric tumors in gp130$^{F/F}$ knock-in mutant mice (Tebbutt et al., 2002), which spontaneously develop gastric adenomas by 4–5 wk of age that resemble intestinal-type gastric cancer in humans

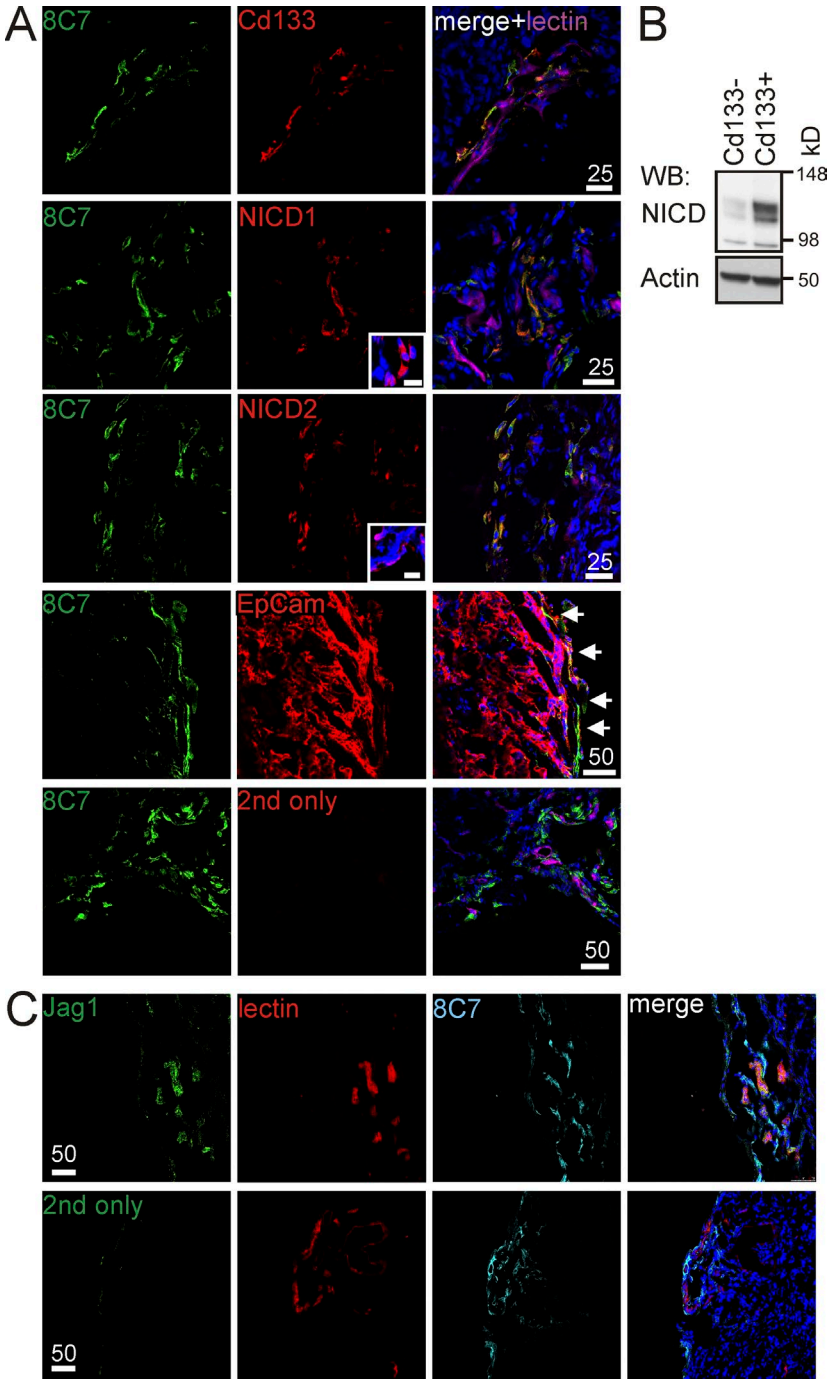

Figure 5. **8C7-recognized, active ADAM10 preferentially marks cancer stem-like cells with active Notch signaling.** (A) LIM1215 tumor sections from mice injected once with Alexa^{647} 8C7 (100 µg, sub-therapeutic dose) and rhodamine-lectin were costained with antibodies against the tumor stem cell marker CD133 or against cleaved (active) Notch1 or Notch2 intracellular domains (NICD1,2), or EpCam. Dark blue indicates nuclear stain. Insets show high-magnification images of tumors from control, non-8C7-injected mice showing specificity of NICD staining and colocalization with nuclear stain; inset bars, 10 µm. Arrows indicate colocalization of 8C7 and EpCam staining. (B) Dispersed tumor cells were sorted for CD133 expression by FACS, and lysates from equal numbers of CD133$^{+/-}$ cells were analyzed by WB for active Notch1 (NICD1). (C) Tumor sections from A were costained for Notch ligand Jagged1. Data are representative of at least two independent experiments. (A and C) Scale bars are in micrometers.

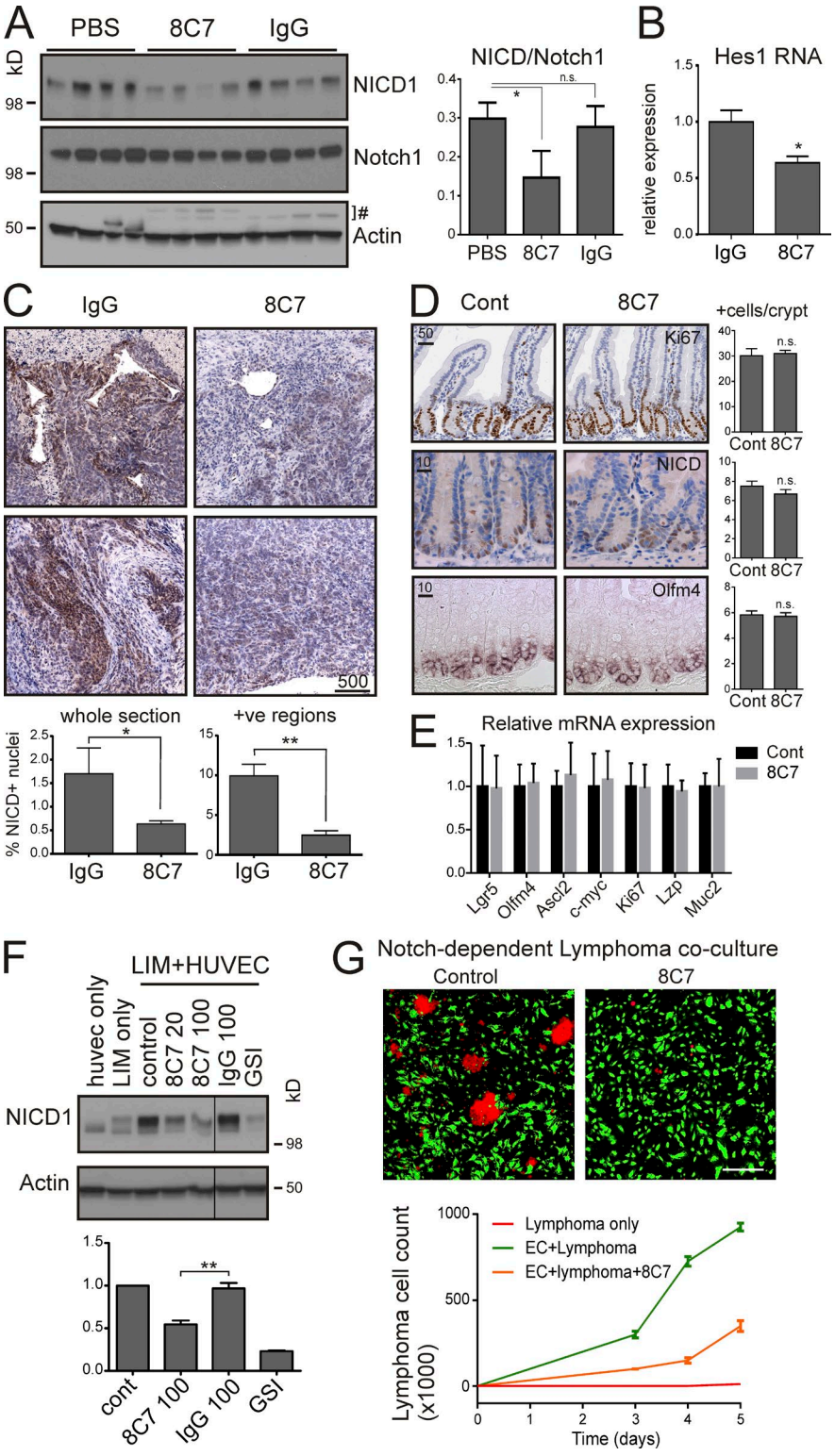

Figure 6. **8C7 inhibits Notch signaling in tumor cells.** (A) Protein extracts of LIM1215 tumors from mice (n = 4) treated for 3 wk with PBS (control) or 8C7 or control IgG (67 mg/kg) were analyzed by WB with antibodies against NICD or actin as loading control (# IgG bands). Graph shows quantitation of NICD level relative to Notch1 (n.s., nonsignificant). (B) RNA extracts of LIM1215 tumors from the mice treated as in A were analyzed by real-time PCR for expression of Notch target Hes1 (normalized to averaged control). (C) Tumors from mice (n = 3) treated as in A were stained with anti-NICD1 antibody, and positive nuclei counts from whole tumor sections or regions (~10/section) of positive staining were quantified. Images show representative areas of positive staining, including around vessel-like structures. Graphs in A–C show mean ± SEM (n = 4); *, $P < 0.05$; **, $P < 0.01$ by unpaired two-tailed Student's t test. (D) Proximal small intestine from vehicle control and 8C7-treated mice (n = 7) was analyzed for expression of Ki67 and NICD (by IHC) and for Olfm4 (by in situ hybridization). (C and D) Scale bars are in micrometers. (E) Quantitative PCR analysis of RNA extracts from small intestine of mice as in D, showing expression (relative to average control) of the indicated markers. (D and E) Graphs show mean ± SEM (n = 7); n.s., nonsignificant by unpaired two-tailed Student's t test. (F) Tumor cells recovered from LIM1215 tumor xenografts were sorted for negative anti-CD133 staining and maintained in culture. HUVECs were then added for 30 min in the presence of 8C7 (20 or 100 µg/ml), control IgG (100 µg/ml), GSI (10 µM), or vehicle control. Cell lysates were recovered and analyzed by WB as indicated. Black lines indicate that intervening lanes have been spliced out. Graph shows levels of active Notch1 (NICD1) relative to control (mean ± SEM; **, $P < 0.01$ by unpaired two-tailed Student's t test [8C7 vs. control IgG]; n = 3 experiments). (G) 8C7 inhibits Notch-dependent lymphoma cell proliferation. Co-cultures of lymphoma cells isolated from Eμ-Myc mice (red) and E4ORF1-transduced HUVECs expressing Jagged1 (ECs, green) were grown in serum-free conditions in the presence of 5 µg/ml 8C7 or control IgG for 5 d and counted over time. Lymphoma cells cultured alone serve as control for dependence on ECs (red line; n = 3). Bar, 50 µm.

(Thiem et al., 2013) and are reminiscent of the spontaneously arising Notch-dependent intestinal tumors in mice expressing a constitutively active gp130 receptor (Taniguchi et al., 2015). Consistent with our previous data in xenografts and human tumors, analysis of tissue extracts from $gp130^{F/F}$ mice revealed expression of HMW ADAM10 within the emerging adenomas as well as the adjacent epithelium of the glandular stomach (antrum), but not in age-matched WT mice

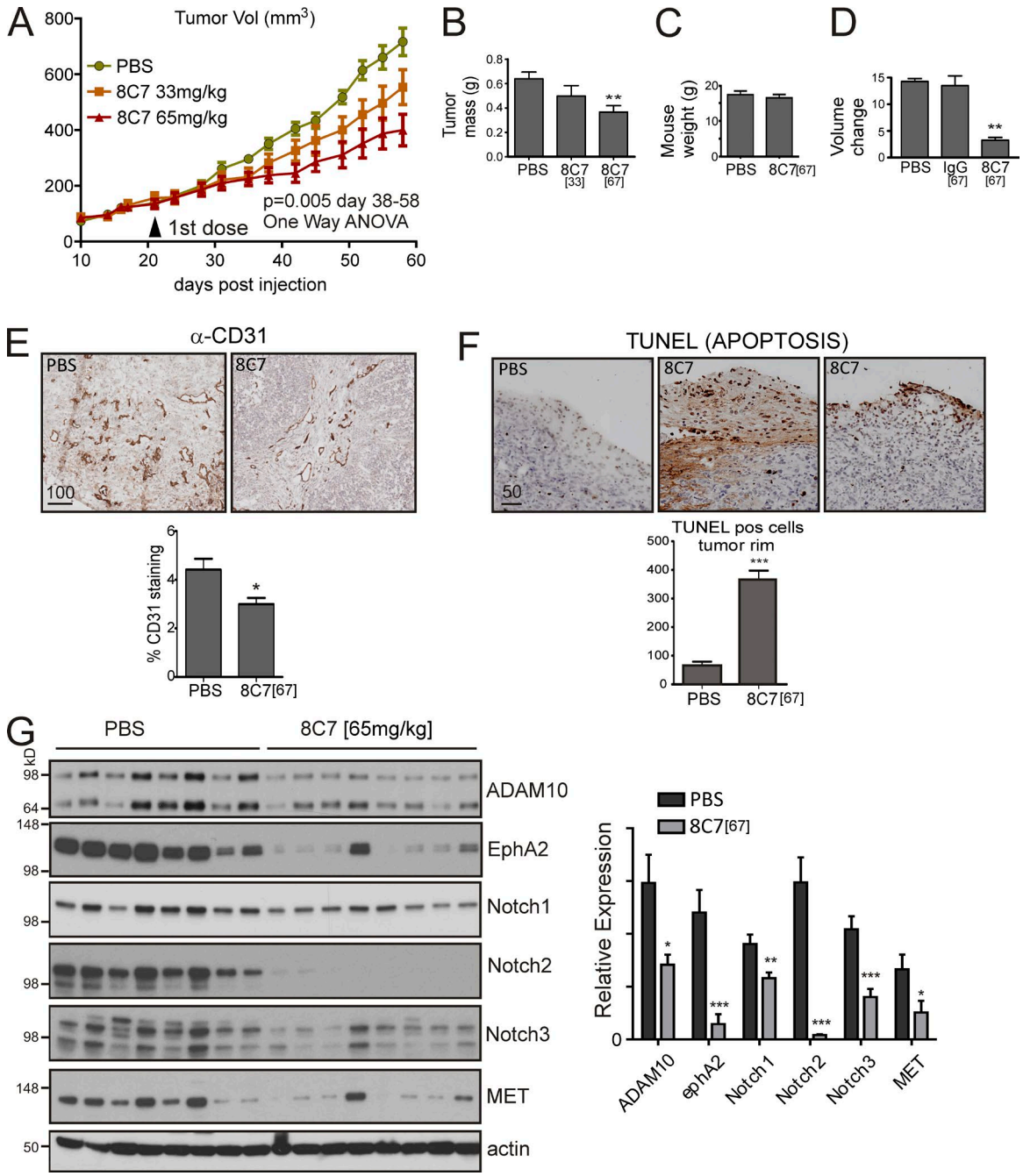

Figure 7. **8C7 inhibits growth of LIM1215 tumors in mice.** (A–C) Mice bearing LIM1215 human tumors were treated with 8C7 mAb (33 or 67 mg/kg) or PBS control (n = 8). (A) Tumor volumes. (B) Final tumor mass. (C) Final mouse weights. (D) Repeat experiment as in A with 67 mg/kg 8C7 or an isotype-matched control mAb (IgG) shows the specific effect of 8C7 (n = 3). (E) Staining of endothelial cells (α-CD31) shows reduced vascularity in 8C7-treated tumors. (F) TUNEL staining of tumors shows increased apoptosis after 8C7 treatment, especially at the vascularized tumor rim. (E and F) Scale bars are in micrometers. (G) WB analysis of lysates from individual tumors (eight/treatment) shows down-regulation of Notch receptors, EphA2, and MET in 8C7-treated tumors. Graphs show mean ± SEM; *, P < 0.05; **, P < 0.01; ***, P < 0.001 by two-tailed Student's t test (8C7 vs. PBS). Data are representative of three independent experiments.

(Fig. 8 A). Treatment of 3-wk-old gp130$^{F/F}$ mice for 5 wk with 8C7 reduced gastric tumor burden, without any effect on spleen or mouse weight (Fig. 8 B). Immunohistochemical analysis revealed significantly lower levels of active Notch (NICD) in the tumors (Fig. 8 C), and RT-PCR analysis of RNA extracts showed decreased levels of the Notch target

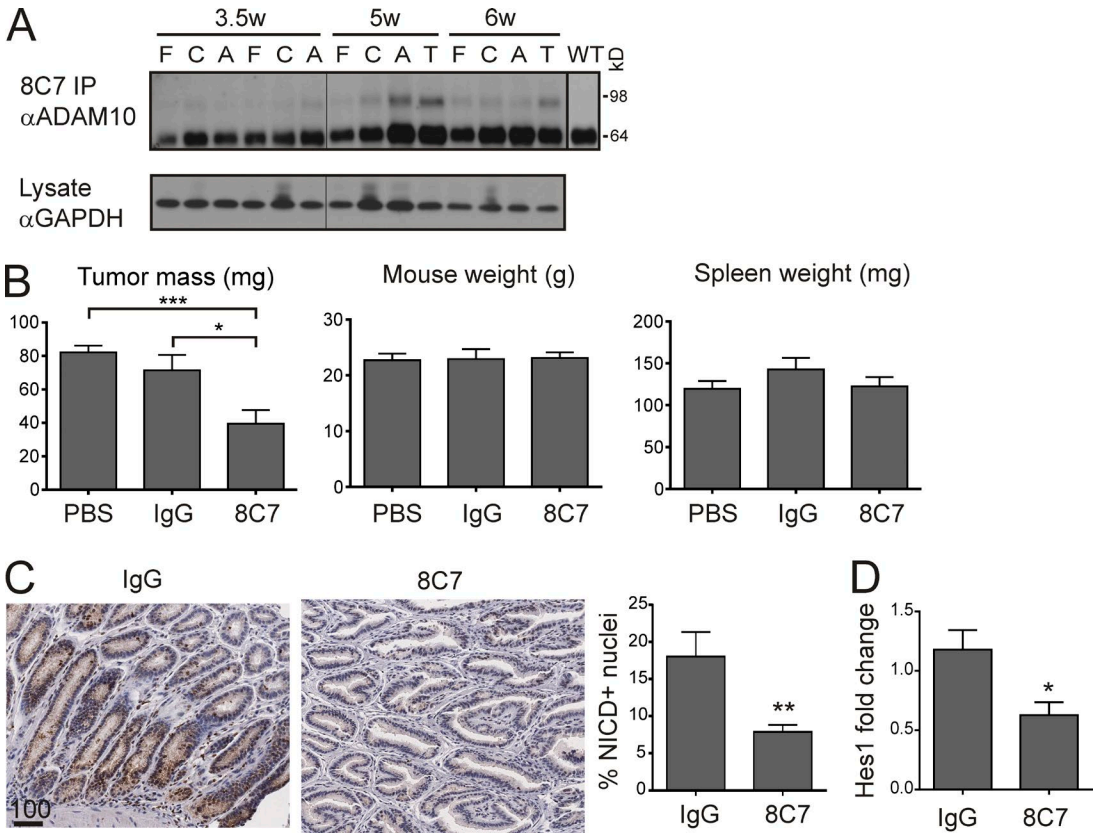

Figure 8. **8C7 inhibits spontaneous tumor growth in gp130$^{F/F}$ knock-in mice.** (A) 8C7 immunoprecipitates of ADAM10 from stomach tissues from gp130$^{F/F}$ knock-in mice that develop spontaneous gastrointestinal tumors at 5–6 wk of age. Samples from different parts of the stomach are shown; F, fundus; C, corpus; A, antrum; T, tumor. Note the appearance of HMW ADAM10 at 5–6 wk, but not in WT mice (6 wk). (B) Mice were treated twice/week from 3 wk of age with 8C7 (n = 10), PBS (n = 9), or control IgG (n = 7), using littermates from four individual experiments. Tumor burden, mouse weight, and spleen weight were assessed at 8 wk. Graphs show mean ± SEM. (C) Tumor sections from 8C7- or control IgG–treated mice (n = 4) were analyzed by staining for active notch (NICD1). Graph shows mean ± SEM using 10 images/treatment. Scale bar is in micrometers. (D) RT-PCR analysis of Hes1 in tumors from gp130$^{F/F}$ mice treated with 8C7 or control IgG (mean ± SEM, n = 4) normalized to PBS treated. For all graphs, *, P < 0.05; **, P < 0.01; ***, P < 0.001 by unpaired, two-tailed Student's t test.

Hes1 (Fig. 8 D), consistent with the effects of 8C7 that we observed in the LIM1215 colorectal tumor xenografts.

CSCs maintained by Notch signaling are thought to contribute to tumor chemoresistance, as well as metastasis and EMT (Espinoza et al., 2013; Giancotti, 2013). Because active ADAM10 specifically marks these cells in LIM1215 xenografts, we therefore tested 8C7 treatment of this model in combination with Irinotecan, a chemotherapeutic used clinically for CRC. Although established xenograft tumors initially regressed during treatment with Irinotecan, they started to grow back ("relapsed") after treatment. However, 8C7 co-treatment inhibited this relapse and caused complete regression in ∼40% of tumors, indicating that 8C7 effectively inhibited tumor cells resistant to chemotherapy (Fig. 9, A and B). Consistent with this, staining for the CD133 stem cell marker revealed fewer CD133^{+} cells in the remaining tumors when compared with tumors of control mice (Fig. 9 C), further supporting the notion that 8C7-directed binding of active ADAM10 targets chemo-resistant tumor stem cells.

Lastly, although 8C7 clearly inhibits signaling by notch, and also Eph receptors (Atapattu et al., 2012), the antibody does not interact directly with residues identified as contributing to substrate binding (Fig. 3; Janes et al., 2005), raising the question of its mechanism of inhibition. Indeed, comparison of 8C7 and control ADAM10 (4A11) immunoprecipitates shows that rather than inhibiting substrate binding, 8C7-bound ADAM10 preferentially binds interacting substrates, including Notch receptors (Fig. 10 A). To understand the mechanism of inhibition, in the absence of a full-length structure of ADAM10 we compared our 8C7-bound ADAM10 D+C structure with available full-length structures of snake venom MPs, which contain a similar overall M+D+C domain architecture and primary sequence cysteine patterns similar to that of the mammalian ADAMs (Takeda et al., 2006; Guan et al., 2010). Interestingly, these show an overall C-shaped structure, with a flexible linker between the MP and the D+C protein regions, such that the MP domain resides within the concave site of the D+C

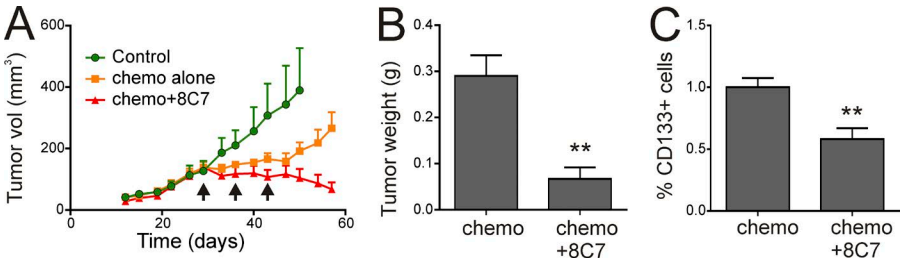

Figure 9. **8C7 is most effective in combination with chemotherapy.** (A) Tumor volumes of LIM1215 tumor xenografts treated with Irinotecan (three injections, arrows) alone (orange), or with continued 8C7 treatment (red, 1 mg), or PBS alone (green). Graph shows mean tumor volumes (with SEM) measured over time ($n \geq 5$). (B) Weight of tumors recovered from mice in A. (C) The percentage of $CD133^+$ cells in tumors recovered from mice treated as in A ($n \geq 5$) was assessed by FACS with anti-CD133 antibodies. (B and C) Graphs show mean ± SEM; **, $P < 0.01$ by unpaired two-tailed Student's *t* test. Data are representative of three independent experiments.

region. Assuming the mammalian ADAMs have a similar overall architecture, binding of 8C7 to the ADAM10 D+C region would compete with the MP domain for its position close to the substrate binding C domain (Fig. 10 B). This notion is supported by our previous finding that 8C7 binds the isolated ADAM10 C domain with higher affinity compared with the full-length ECD (Atapattu et al., 2012). Displacement of the MP domain relative to bound substrate would also explain how 8C7-bound ADAM10 can have high activity against soluble peptide substrate in vitro, able to access the active site, but is blocked from cleaving membrane-bound substrates in a cellular or tissue context.

DISCUSSION

ADAM10 is a recognized therapeutic target, along with ADAM17, and inhibitors of their activity are of great interest for treatment of inflammatory diseases and cancer, although previous small molecule inhibitors targeting the MP domain have not successfully translated to the clinic (Saftig and Reiss, 2011). There is thus a need for alternative approaches to inhibit ADAM activity. We previously identified the cysteine-rich membrane proximal domain of ADAM10 as responsible for substrate recognition (Janes et al., 2005), suggesting an alternative target. This domain in ADAM17 is also implicated in activity-related conformational change through shuffling of disulfide linkages with a conserved thioredoxin CxxC motif, which is conserved in ADAM10 and lies adjacent to the substrate-binding domain (Janes et al., 2005). Thus, ADAM17 activity is inhibited by mutation of the CxxC motif and is regulated by modulating redox conditions (Wang et al., 2009) and activity of PDI (Willems et al., 2010), which catalyzes disulfide bond switching. In support, PDI modulates both activity of ADAM17 and its apparent conformation (Willems et al., 2010), and a recent nuclear magnetic resonance study shows two distinct, PDI-regulated conformations of bacterially expressed ADAM17, with

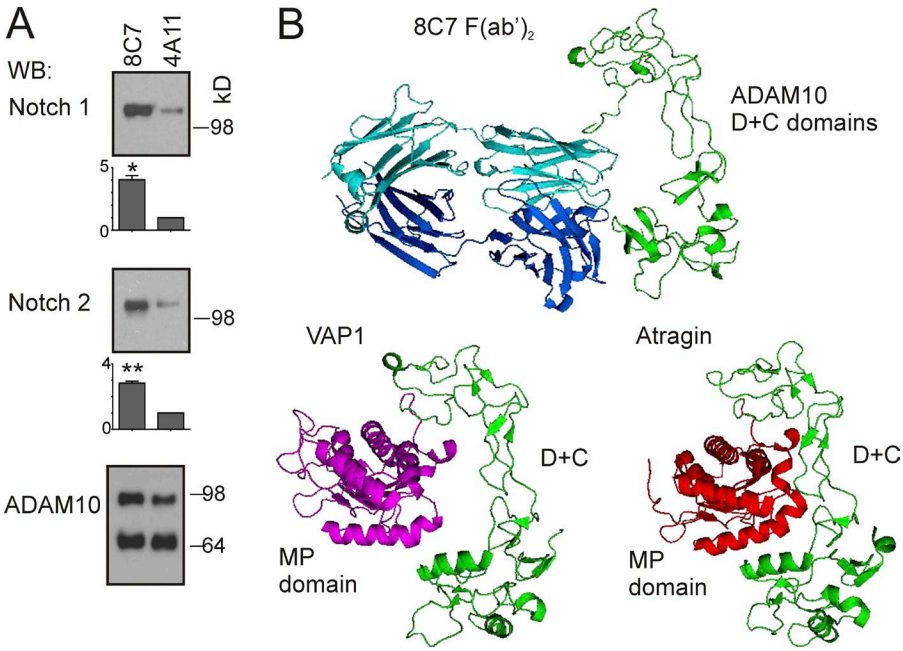

Figure 10. **8C7 does not inhibit ADAM10 substrate binding but likely displaces its MP domain.** (A) 8C7-bound ADAM10 shows preferential association with Notch receptor substrates. IPs from LIM1215 lysates with 8C7 and 4A11, equalized for ADAM10 levels by WB, were blotted with antibodies against the indicated proteins. Graphs show ratio between coprecipitated proteins and levels of total ADAM10 quantitated by densitometry (mean ± SEM from three independent experiments; *, $P < 0.05$; **, $P < 0.01$ by one-sample Student's *t* test relative to 4A11 binding). (B) Comparison of 8C7/ADAM10 D+C structure with full-length structures of related snake venom MPs shows similar positioning of MP domains compared with 8C7 binding, indicating likely competition.

distinct CxxC linkages, although the activities of the two forms or their relevance for mammalian-expressed ADAM17 were not assessed (Düsterhöft et al., 2013).

We now show that a distinct, active form of ADAM10 is specifically identified by our antibody, 8C7. This conformation of the ADAM10 substrate-binding domain is dependent on CxxC bonding because 8C7 binding is blocked by CxxC mutation and is altered by modulating the redox environment. Furthermore, our determination of the structure of 8C7 in complex with ADAM10 shows binding to C639, which is disulfide-bonded to C594 in the CxxC motif. Our data show the 8C7-recognized conformation is active because 8C7 immunoprecipitates of ADAM10 showed marked enrichment of protease activity, and oxidative conditions, known to enhance ADAM activity, correlated with increased 8C7 binding. Experiments are underway to define the disulfide bonding pattern and structure of the presumed alternate, inactive ADAM10 domain conformation.

Importantly, the selectivity of 8C7 for active ADAM10 allowed identification of an active ADAM10 population that preferentially marks tumors compared with normal tissues in both mouse models and in human tumor samples. Interestingly, the 8C7-recognized form of ADAM10 that was specific to tumors was associated with the increased presence of an HMW, unprocessed form, which we confirmed is present on the cell surface and is cleavable by furin. Although the ADAM10 Pro domain can have an inhibitory function, such as when the recombinant domain is applied exogenously to cells (Moss et al., 2007), it also has an essential chaperone function (Anders et al., 2001), and ADAM10 Pro domain mutations that likely disrupt this function have recently been shown to attenuate ADAM10 activity in late-onset Alzheimer's disease (Suh et al., 2013). Reversible activation of unprocessed ADAM17 has also recently been demonstrated (Le Gall et al., 2010), so it is likely the unprocessed ADAM10 prevalent in tumors is similarly readily activated, as indicated by the high degree of activity in tumors. This activity is most likely supported by high levels of ROS in the tumor microenvironment (Benz and Yau, 2008), favoring the active ADAM10 isomer. The prevalence of unprocessed ADAM10 in tumors has not previously been reported, and the cause is unknown; however, reduced processing of other membrane-bound proteins and altered activity of pro-protein convertases are known to occur in cancer cells (Sadeqzadeh et al., 2011; Huang et al., 2012; Demidyuk et al., 2013). Indeed, inhibited processing may also be ROS related, as oxidation of furin disrupts its calcium-binding capacity, resulting in defective activity (Spencer et al., 2008). Thus, high ROS levels may result in coincident activation of ADAM10 with inhibition of its processing by furin, rather than activity being directly dependent on processing.

Notably, although 8C7 bound to the tumor mass, it was clearly most strongly bound to a distinct population of cells within tumors that were closely associated with blood vessels and that express the CSC marker CD133. A recent study has described $CD133^+$ cells in perivascular regions of human CRC, which display elevated Notch signaling as the result of ADAM17-mediated release of the ligand Jagged-1 from endothelial cells (Lu et al., 2013). In agreement, we find 8C7-targeted $CD133^+$ cells show high levels of NICD1 and 2, both by IF staining of tumors and by analysis of $CD133^+$ sorted cells by WB. This suggests that the 8C7-recognized, active ADAM10 particularly marks a subpopulation of tumor cells previously identified as having a CSC phenotype. Interestingly, CSCs are protected from ROS toxicity by expression of aldehyde dehydrogenase (ALDH), enabling them to maintain high levels of ROS (Raha et al., 2014). Indeed, we also find 8C7-bound cells recovered from tumors showed markedly higher ROS levels compared with unbound (8C7 negative) cells, suggesting a likely explanation for high ADAM10 activity and 8C7 binding of these cells. Interestingly, normal intestine is also known to contain elevated NOX1 and ROS levels, important in Notch- and Wnt-dependent homeostasis and thought to act via PTEN/Akt signaling (Coant et al., 2010). The lack of significant effects of 8C7 in the intestine suggests the selectivity of 8C7 for tumors may reflect distinct localization and/or levels of ROS production (known to result from deregulated RTK signaling in tumors and to be highly compartmentalized [Jin et al., 2010; Woo et al., 2010]) and/or overexpression of unprocessed ADAM10 on the cell surface in tumors. There may also be differing expression of other associated proteins that regulate ADAM10 in these tissues, which will be important to investigate in the future.

Importantly, the significant inhibition of Notch-dependent signaling by 8C7 in vitro and in tumors is correlated with inhibition of tumor growth in vivo. Consistent with Notch inhibition, treated tumors showed decreased vascularity and expression of Notch receptors and other downstream targets. Notch signaling in CSCs is believed to contribute to tumor initiation and maintenance and to mediate chemoresistance, and indeed we find 8C7 inhibition was most effective in tumors treated with chemotherapy (Irinotecan), suggesting targeting of chemo-resistant cells. In support, $CD133^+$ CSCs were selectively reduced by 8C7 compared with chemotherapy alone. Although Notch is a key substrate, ADAM10 also regulates signaling by RTKs including MET, Eph, and EGFR/erbB receptors (Sahin et al., 2004; Saftig and Reiss, 2011). We show MET and EphA2 were also markedly reduced after 8C7 treatment, which may reflect a direct effect on signaling and/or their coordinated transcriptional regulation in stem cells (Finkbeiner et al., 2009; Gucciardo et al., 2014), which are depleted by 8C7 treatment. We also noted reduction of EGFR levels that was more variable (unpublished data), possibly caused by compensatory roles of other ADAMs such as ADAM17 (Sahin et al., 2004). Together, this suggests tumor growth inhibition by 8C7 may reflect its action on multiple signaling pathways, which is an important area for further investigation.

In conclusion, we describe a novel active form of ADAM10 prevalent in tumors, particularly in tumor stem-like cells with active Notch, which is selectively recognized by our

antibody 8C7. This selectivity of 8C7 for active ADAM10, its inhibition of Notch activity, and its efficacy in inhibiting tumor growth, particularly after chemotherapy, indicate considerable potential for its development as a novel therapeutic.

MATERIALS AND METHODS

Cell culture and reagents

Human colorectal carcinoma cell lines (from J. Mariadason, Olivia Newton-John Cancer Research Institute, Austin Health, Heidelberg, Victoria, Australia) were maintained in RPMI 1640/10% FCS in 10% CO_2/90% air. ADAM10$^{-/-}$ mouse embryonic fibroblasts (Hartmann et al., 2002) were maintained in DMEM 10% FCS in 5% CO_2/95% air atmosphere. Commercial ADAM10 antibodies were as follows: R&D Systems MAB1427 (anti-human, for IP) or MAB946 (mouse/human, for IF); Abcam pAb 39177 (C terminus, for WB and IP) or pAb 39178 (Pro-domain, for WB). Other commercial antibodies used were from Cell Signaling Technologies (Notch1-3, NICD1, EphA2, MET, Jagged1, erbB2, and GAP DH), Abcam (PDI), EMD Millipore (NICD2), Novus Biologicals (EGFR), BioLegend (FITC–anti-EpCam), eBioscience (FITC–anti-CD133), and Thermo Fisher Scientific (actin).

Mouse experiments

Athymic mice (BALB/c nude, 5–6 wk old; male) were from Animal Resources Centre (Canning Vale, Western Australia, Australia). All animals were handled in strict accordance with good animal practice as defined by the National Health and Medical Research Council (Australia) Code of Practice for the Care and Use of Animals for Experimental Purposes, and experimental procedures were approved by the Monash Animal Research Platform Animal Ethics Committee. 7×10^6 LIM1250 cells in 200 µl PBS/30% growth factor reduced Matrigel (BD) were injected subcutaneously in the mouse flanks. When tumor volumes reached 75–150 mm^3 (measured by calipers, volume = [length × width^2]/2), mice were treated twice weekly by i.p. injection with either PBS, 8C7, or IgG1κ isotype-matched control antibody as indicated. Irinotecan-HCl (Selleck Chemicals) was prepared as described previously (Zamboni et al., 1998) and diluted to 1.1 mg/ml in PBS for i.p. injection (7.5 or 15 mg/kg [Fischer et al., 2011]). Tumors and tissues were recovered for protein analysis, imaging by IF microscopy, IHC, or flow cytometry.

For the gp130$^{F/F}$ spontaneous stomach tumor model (Tebbutt et al., 2002), mice were treated twice weekly from 3.5 wk old with 65 mg/kg 8C7, or isotype-matched control antibody, or PBS only. After 5 wk, stomach tissues were recovered, polyps were excised and weighed, and tissue was snap frozen for analysis by IF/IHC (OCT sections) or WB of protein extracts. WT c57/b6 mice were used as control.

IP and Western blotting

Cultured cells were lysed as described previously (Janes et al., 2011). For protein analysis of tumors and tissues, tissue was homogenized (50 mg/ml) in RIPA buffer (50 mM Tris-HCl, pH 7.4, 150 mM NaCl, 1% Triton X-100, 0.5% sodium deoxycholate, 0.1% SDS, 1 mM EDTA, and protease inhibitors), and protein concentration was determined by BCA assay (Thermo Fisher Scientific). 20 µg of total lysates or immunoprecipitates from 100 µg of lysates was analyzed by SDS-PAGE and WB. IP was with ADAM10 mAbs coupled to Mini-Leak beads (10 µl/sample; KemEnTec) or with soluble 8C7 or anti-ADAM10 pAb (Abcam pAb 39177) followed by protein A Sepharose (GE Healthcare). ADAM10 was detected on WBs with Abcam pAb 39177 and anti–rabbit-HRP secondary antibodies and visualized using an ECL substrate (SuperSignal; Thermo Fisher Scientific). Frozen human tissue samples (colon adenocarcinomas and matched normal colon) were from surgical biopsies taken between 1995 and 2007, provided by C. Murone at the Austin Health Tissue Bank.

For modulation of redox conditions, LIM1215 CRC cells at 80% confluence were starved in serum-free RPMI overnight. Cells were treated for 1 h at 37°C with 1 mM DTT, 1–40 mM H_2O_2, 1 µg/ml EGF, and EphrinA5-Fc (1.5 µg/ml) precross-linked with anti–human IgG (Janes et al., 2011). Treated cells were washed in PBS and lysed, and total protein levels were determined. Equal protein levels were incubated with either 8C7–Mini-Leak beads or 4A11–Mini-Leak beads and subjected to WB to determine which ADAM10 levels bind to each antibody under the aforementioned treatments.

For furin treatments, washed 8C7 and 4A11 IPs from LIM1215 CRC cell lysates were treated with 2 U/100 µl furin (New England Biolabs, Inc.) in buffer specified by the supplier (100 mM Hepes, pH 7.5 [at 25°C], 0.5% Triton X-100, and 1 mM $CaCl_2$) at 37°C.

ADAM MP activity assay

ADAM10 was pulled down by IP from lysates of LIM1215 colon carcinoma cells or human colorectal tumors using 8C7 and 4A11 coupled to Mini-Leak beads. Immunoprecipitates pre-equalized for overall ADAM10 levels (by WB) were incubated with Mca-PLAQAV-Dpa-RSSSR-NH2 fluorogenic peptide substrate (R&D Systems), 10 µM in PBS at 37°C for 1 h. Antibody-conjugated beads were incubated with substrate as control. Substrate supernatants were analyzed using a FLUOstar OPTIMA (BMG Labtech) plate reader at 320-nm excitation and 405 emission wavelengths, and low level bead-only background fluorescence was subtracted from sample readings.

Mutagenesis and PCR analysis

ADAM10 CxxC mutant: AxxA point mutation was introduced to human ADAM10-myc (OriGene) by site-directed mutagenesis (QuikChange XL; Agilent Technologies) by introducing alanines at Cys594 and Cys597. Mutants verified by sequencing were transfected into ADAM10$^{-/-}$ MEFs using X-treme transfection reagent (Roche), and expression was confirmed by WB and IF microscopy.

cDNA from RNA extracts (QIAGEN RNeasy) of snap frozen tumors were analyzed by quantitative PCR using iTaq SYBR green (Bio-Rad Laboratories) and a RotorGene 3000 cycler (Corbett Research). Primers specific for human or mouse Hes1 or the indicated mouse genes (Fig. 6 F; Horvay et al., 2015) were used to determine expression relative to housekeeping genes β-actin and tubulin by comparative C_T ($\Delta\Delta C_T$).

Tissue IHC and IF

Tissues were OCT embedded (Tissue-TEK), sectioned (6 µm), and fixed (10 min, acetone) or formalin fixed, paraffin embedded, and sectioned. For IHC, Vector Laboratories ABC secondary antibody staining kit was used to detect the bound primary antibodies. Sections were counterstained with hematoxylin and imaged on a Leica Aperio scanner. Quantitation (positive nuclei) was performed using Aperio ImageScope software, taking the average from 10–20 images/point. Olfm4 in situ hybridization was performed as previously described (Horvay et al., 2015), and + cells counted manually in bisected crypts. Displayed images of intestinal NICD IHC and Olfm4 in situ hybridization were taken on a ZEISS AxioVision microscope. For IF, frozen (OCT) sections were incubated with fluorescent-conjugated antibodies or unconjugated primary followed by Alexa-labeled secondary antibodies. Nuclei were counterstained with Hoechst, and slides mounted with Fluoromount (SouthernBiotech) for imaging on a Leica SP5 confocal microscope.

Flow cytometry

Single cell suspensions were made from LIM1215 tumors by digesting finely chopped tumor pieces with Collagenase Type 3/Deoxyribonuclease I (Worthington Biochemical Corporation) in HBBS (Invitrogen, 1 h, 37°C), filtering through successive 40-µm and 20-µm sieves and treatment with red blood cell lysing buffer (Sigma-Aldrich). Cells were labeled with conjugated anti-CD133 (Miltenyi Biotec) and analyzed/sorted by FACS (LSRII or Influx flow cytometers; BD). Dead cells were detected with propidium iodide. Subsequent analysis was with FlowJo software (Tree Star).

Detection of ROS in tumor cell isolates

Tumors from mice injected with Alexa-labeled 8C7 (100 µg) were recovered, and cell suspensions were prepared and analyzed by flow cytometry. FACS-sorted 8C7-bound/unbound tumor cells were tested using a reaction mix that included 50 µM Amplex Red (Invitrogen) and 0.1 U/ml HRP (Invitrogen) in Krebs-Ringer phosphate. 20 µl of 8C7-bound tumor cells (a total of 5×10^4) was added to 100 µl of the prewarmed reaction mixture and incubated for 1 h at 37°C. A microplate reader (CLARIOstar, BMG Labtech) was used to measure fluorescence (excitation 530–560 nm and emission peak 590 nm).

Crystallization experiments

A bovine ADAM10 fragment containing disintegrin and cysteine-rich domains (ADAM10 (D+C), residues 455–646) was produced as described previously (Janes et al., 2005). The 8C7 $F(ab')_2$ fragment was prepared by digesting 8C7 with pepsin at pH 3.0 (enzyme/substrate ratio 1:100) for 2 h at room temperature, terminated by raising the pH to 8.0. The final purification was performed using gel filtration chromatography (SD-200 column, 20 mM Hepes, and 150 mM NaCl, pH 7.5). The protein eluted as a monomer of ∼110 kD.

For crystallization, ADAM10 (D+C) was mixed with $F(ab')_2$ at 2:1 molar ratio (final concentration 20 mg/ml) in a buffer containing 20 mM Hepes and 150 mM NaCl, pH 7.5. The complex was crystallized in a hanging drop by vapor diffusion at room temperature against a reservoir containing 0.1 M Hepes, 0.2 M NaCl, and 1.6 M ammonium sulfate. Sizeable crystals, in the space group P212121, grew after 2 mo but could be reproduced in 2–3 d using the additive 30% 1,4-Dioxane. The structure was determined using molecular replacement with the ADAM10 (D+C) structure and a $F(ab')_2$ structure as search models (PDB IDs 2AO7 and 1K4D, respectively). The ADAM10/mAb structure model was built with program Coot and refined with PHENIX_Refine. The final structure was validated with PROCHECK.

Online supplemental material

Table S1 shows data collection and refinement statistics from the crystal structure of the ADAM10 D+C domain/8C7 $F(ab')_2$ complex. Online supplemental material is available at http://www.jem.org/cgi/content/full/jem.20151095/DC1.

ACKNOWLEDGMENTS

This manuscript is dedicated to our friend and colleague Martin Lackmann, November 3, 1956 to May 22, 2014, who is sadly missed.

We are grateful to Monash Micro Imaging and Monash Flowcore for technical support and to A. Perani, C. Murone, and J. Mariadason (Olivia Newton-John Cancer Research Institute, Austin Health, Heidelberg, Victoria, Australia) for antibody production, human tissue samples, and CRC cell lines, respectively.

This work was supported by National Health and Medical Research Council (NHMRC), Australia (grants 384242, 1067609, and 1093304; fellowships to P.W. Janes [384285], M. Lackmann [1003908], M. Ernst [1079257], and A.M. Scott [1084178]; and scholarship to L. Atapattu [1017654]) and by funds from the Operational Infrastructure Support Program provided by the Victorian Government, Australia. Additional funding included an award to D.B. Nikolov from The Experimental Therapeutics Center of Memorial Sloan-Kettering, support from Mr. William H. and Mrs. Alice Goodwin and the Commonwealth Foundation for Cancer Research, and National Institutes of Health grants R21CA185930 and R01 NS03848 (to D.B. Nikolov). x-ray diffraction experiments were conducted remotely at the Advanced Photon Source on the Northeastern Collaborative Access Team beamlines ID24, which are supported by a grant from the National Institute of General Medical Sciences (P41 GM103403) from the National Institutes of Health. Use of the Advanced Photon Source, an Office of Science User Facility operated for the US Department of Energy (DOE) Office of Science by Argonne National Laboratory, was supported by the US DOE under contract no. DE-AC02-06CH11357.

Data presented here are relevant to patent applications US 61/935552 and US 7,960,513. The authors declare no additional competing financial interests.

Author contributions: Experiments were performed by L. Atapattu, C. Chheang, P.W. Janes, and M.E. Vail, with support by L. Hii and C. Llerena. Olfm4 in situ was performed with help from K. Horvay and H.E. Abud. Crystallization experiments and analysis were performed by N. Saha, K. Xu, and D.B. Nikolov. Notch-dependent lymphoma assay

was performed by B.-S. Ding, Z. Cao, and S. Rafii. Mass spectrometry analysis was performed by U. Kusebauch and R.L. Moritz. gp130$^{F/F}$ mouse experiments were performed by M.F. Eissman and M. Ernst, with analysis by P.W. Janes and C. Chheang. Antibody production and mAb 4A11 generation were performed by Z. Liu and A.M. Scott. The project was conceived and directed by P.W. Janes and M. Lackmann. The manuscript was written by P.W. Janes, M. Lackmann, L. Atapattu, N. Saha, and D.B. Nikolov.

Submitted: 2 July 2015
Accepted: 28 June 2016

REFERENCES

Anders, A., S. Gilbert, W. Garten, R. Postina, and F. Fahrenholz. 2001. Regulation of the alpha-secretase ADAM10 by its prodomain and proprotein convertases. *FASEB J.* 15:1837–1839.

Atapattu, L., N. Saha, C. Llerena, M.E. Vail, A.M. Scott, D.B. Nikolov, M. Lackmann, and P.W. Janes. 2012. Antibodies binding the ADAM10 substrate recognition domain inhibit Eph function. *J. Cell Sci.* 125:6084–6093. http://dx.doi.org/10.1242/jcs.112631

Atapattu, L., M. Lackmann, and P.W. Janes. 2014. The role of proteases in regulating Eph/ephrin signaling. *Cell Adh. Migr.* 8:294–307. http://dx.doi.org/10.4161/19336918.2014.970026

Benham, A.M. 2012. The protein disulfide isomerase family: key players in health and disease. *Antioxid. Redox Signal.* 16:781–789. http://dx.doi.org/10.1089/ars.2011.4439

Benz, C.C., and C. Yau. 2008. Ageing, oxidative stress and cancer: paradigms in parallax. *Nat. Rev. Cancer.* 8:875–879. http://dx.doi.org/10.1038/nrc2522

Cao, Z., B.-S. Ding, P. Guo, S.B. Lee, J.M. Butler, S.C. Casey, M. Simons, W. Tam, D.W. Felsher, K. Shido, et al. 2014. Angiocrine factors deployed by tumor vascular niche induce B cell lymphoma invasiveness and chemoresistance. *Cancer Cell.* 25:350–365. http://dx.doi.org/10.1016/j.ccr.2014.02.005

Chiarugi, P., and P. Cirri. 2003. Redox regulation of protein tyrosine phosphatases during receptor tyrosine kinase signal transduction. *Trends Biochem. Sci.* 28:509–514. http://dx.doi.org/10.1016/S0968-0004(03)00174-9

Coant, N., S. Ben Mkaddem, E. Pedruzzi, C. Guichard, X. Tréton, R. Ducroc, J.N. Freund, D. Cazals-Hatem, Y. Bouhnik, P.L. Woerther, et al. 2010. NADPH oxidase 1 modulates WNT and NOTCH1 signaling to control the fate of proliferative progenitor cells in the colon. *Mol. Cell. Biol.* 30:2636–2650. http://dx.doi.org/10.1128/MCB.01194-09

DasGupta, S., P.R. Murumkar, R. Giridhar, and M.R. Yadav. 2009. Current perspective of TACE inhibitors: a review. *Bioorg. Med. Chem.* 17:444–459. http://dx.doi.org/10.1016/j.bmc.2008.11.067

Demidyuk, I.V., A.V. Shubin, E.V. Gasanov, A.M. Kurinov, V.V. Demkin, T.V. Vinogradova, M.V. Zinovyeva, A.V. Sass, I.B. Zborovskaya, and S.V. Kostrov. 2013. Alterations in gene expression of proprotein convertases in human lung cancer have a limited number of scenarios. *PLoS One.* 8:e55752. http://dx.doi.org/10.1371/journal.pone.0055752

Dikic, I., and M.H. Schmidt. 2010. Notch: Implications of endogenous inhibitors for therapy. *BioEssays.* 32:481–487. http://dx.doi.org/10.1002/bies.200900140

Düsterhöft, S., S. Jung, C.W. Hung, A. Tholey, F.D. Sönnichsen, J. Grötzinger, and I. Lorenzen. 2013. Membrane-proximal domain of a disintegrin and metalloprotease-17 represents the putative molecular switch of its shedding activity operated by protein-disulfide isomerase. *J. Am. Chem. Soc.* 135:5776–5781. http://dx.doi.org/10.1021/ja400340u

Espinoza, I., R. Pochampally, F. Xing, K. Watabe, and L. Miele. 2013. Notch signaling: targeting cancer stem cells and epithelial-to-mesenchymal transition. *Onco Targets Ther.* 6:1249–1259. http://dx.doi.org/10.2147/OTT.S36162

Finkbeiner, M.R., A. Astanehe, K. To, A. Fotovati, A.H. Davies, Y. Zhao, H. Jiang, A.L. Stratford, A. Shadeo, C. Boccaccio, et al. 2009. Profiling YB-1 target genes uncovers a new mechanism for MET receptor regulation in normal and malignant human mammary cells. *Oncogene.* 28:1421–1431. http://dx.doi.org/10.1038/onc.2008.485

Fischer, M., W.-C. Yen, A.M. Kapoun, M. Wang, G. O'Young, J. Lewicki, A. Gurney, and T. Hoey. 2011. Anti-DLL4 inhibits growth and reduces tumor-initiating cell frequency in colorectal tumors with oncogenic KRAS mutations. *Cancer Res.* 71:1520–1525. http://dx.doi.org/10.1158/0008-5472.CAN-10-2817

Fischer, O.M., S. Hart, A. Gschwind, N. Prenzel, and A. Ullrich. 2004. Oxidative and osmotic stress signaling in tumor cells is mediated by ADAM proteases and heparin-binding epidermal growth factor. *Mol. Cell. Biol.* 24:5172–5183. http://dx.doi.org/10.1128/MCB.24.12.5172-5183.2004

Fridman, J.S., E. Caulder, M. Hansbury, X. Liu, G. Yang, Q. Wang, Y. Lo, B.B. Zhou, M. Pan, S.M. Thomas, et al. 2007. Selective inhibition of ADAM metalloproteases as a novel approach for modulating ErbB pathways in cancer. *Clin. Cancer Res.* 13:1892–1902. http://dx.doi.org/10.1158/1078-0432.CCR-06-2116

Giancotti, F.G. 2013. Mechanisms governing metastatic dormancy and reactivation. *Cell.* 155:750–764. http://dx.doi.org/10.1016/j.cell.2013.10.029

Groth, C., and M.E. Fortini. 2012. Therapeutic approaches to modulating Notch signaling: Current challenges and future prospects. *Semin. Cell Dev. Biol.* 23:465–472. http://dx.doi.org/10.1016/j.semcdb.2012.01.016

Guan, H.-H., K.-S. Goh, F. Davamani, P.-L. Wu, Y.-W. Huang, J. Jeyakanthan, W.G. Wu, and C.-J. Chen. 2010. Structures of two elapid snake venom metalloproteases with distinct activities highlight the disulfide patterns in the D domain of ADAMalysin family proteins. *J. Struct. Biol.* 169:294–303. http://dx.doi.org/10.1016/j.jsb.2009.11.009

Gucciardo, E., N. Sugiyama, and K. Lehti. 2014. Eph- and ephrin-dependent mechanisms in tumor and stem cell dynamics. *Cell. Mol. Life Sci.* 71:3685–3710. http://dx.doi.org/10.1007/s00018-014-1633-0

Hartmann, D., B. de Strooper, L. Serneels, K. Craessaerts, A. Herreman, W. Annaert, L. Umans, T. Lübke, A. Lena Illert, K. von Figura, and P. Saftig. 2002. The disintegrin/metalloprotease ADAM 10 is essential for Notch signalling but not for α-secretase activity in fibroblasts. *Hum. Mol. Genet.* 11:2615–2624. http://dx.doi.org/10.1093/hmg/11.21.2615

Hartmann, M., A. Herrlich, and P. Herrlich. 2013. Who decides when to cleave an ectodomain? *Trends Biochem. Sci.* 38:111–120. http://dx.doi.org/10.1016/j.tibs.2012.12.002

Hattori, M., M. Osterfield, and J.G. Flanagan. 2000. Regulated cleavage of a contact-mediated axon repellent. *Science.* 289:1360–1365. http://dx.doi.org/10.1126/science.289.5483.1360

Horvay, K., T. Jardé, F. Casagranda, V.M. Perreau, K. Haigh, C.M. Nefzger, R. Akhtar, T. Gridley, G. Berx, J.J. Haigh, et al. 2015. Snai1 regulates cell lineage allocation and stem cell maintenance in the mouse intestinal epithelium. *EMBO J.* 34:1319–1335. http://dx.doi.org/10.15252/embj.201490881

Huang, Y.H., K.H. Lin, C.H. Liao, M.W. Lai, Y.H. Tseng, and C.T. Yeh. 2012. Furin overexpression suppresses tumor growth and predicts a better postoperative disease-free survival in hepatocellular carcinoma. *PLoS One.* 7:e40738. http://dx.doi.org/10.1371/journal.pone.0040738

Janes, P.W., N. Saha, W.A. Barton, M.V. Kolev, S.H. Wimmer-Kleikamp, E. Nievergall, C.P. Blobel, J.P. Himanen, M. Lackmann, and D.B. Nikolov. 2005. Adam meets Eph: an ADAM substrate recognition module acts as a molecular switch for ephrin cleavage in trans. *Cell.* 123:291–304. http://dx.doi.org/10.1016/j.cell.2005.08.014

Janes, P.W., S.H. Wimmer-Kleikamp, A.S. Frangakis, K. Treble, B. Griesshaber, O. Sabet, M. Grabenbauer, A.Y. Ting, P. Saftig, P.I. Bastiaens, and M. Lackmann. 2009. Cytoplasmic relaxation of active Eph controls ephrin shedding by ADAM10. *PLoS Biol.* 7:e1000215. http://dx.doi.org/10.1371/journal.pbio.1000215

Janes, P.W., B. Griesshaber, L. Atapattu, E. Nievergall, L.L. Hii, A. Mensinga, C. Chheang, B.W. Day, A.W. Boyd, P.I. Bastiaens, et al. 2011. Eph receptor function is modulated by heterooligomerization of A and B type Eph receptors. *J. Cell Biol.* 195:1033–1045. http://dx.doi.org/10.1083/jcb.201104037

Jin, H., D.A. Heller, M. Kalbacova, J.H. Kim, J. Zhang, A.A. Boghossian, N. Maheshri, and M.S. Strano. 2010. Detection of single-molecule H2O2 signalling from epidermal growth factor receptor using fluorescent single-walled carbon nanotubes. *Nat. Nanotechnol.* 5:302–309. http://dx.doi.org/10.1038/nnano.2010.24

Kopan, R., and M.X.G. Ilagan. 2009. The canonical Notch signaling pathway: unfolding the activation mechanism. *Cell.* 137:216–233. http://dx.doi.org/10.1016/j.cell.2009.03.045

LaVoie, M.J., and D.J. Selkoe. 2003. The Notch ligands, Jagged and Delta, are sequentially processed by α-secretase and presenilin/γ-secretase and release signaling fragments. *J. Biol. Chem.* 278:34427–34437. http://dx.doi.org/10.1074/jbc.M302659200

Le Gall, S.M., T. Maretzky, P.D. Issuree, X.D. Niu, K. Reiss, P. Saftig, R. Khokha, D. Lundell, and C.P. Blobel. 2010. ADAM17 is regulated by a rapid and reversible mechanism that controls access to its catalytic site. *J. Cell Sci.* 123:3913–3922. http://dx.doi.org/10.1242/jcs.069997

López-Otín, C., and T. Hunter. 2010. The regulatory crosstalk between kinases and proteases in cancer. *Nat. Rev. Cancer.* 10:278–292. http://dx.doi.org/10.1038/nrc2823

Lu, J., X. Ye, F. Fan, L. Xia, R. Bhattacharya, S. Bellister, F. Tozzi, E. Sceusi, Y. Zhou, I. Tachibana, et al. 2013. Endothelial cells promote the colorectal cancer stem cell phenotype through a soluble form of Jagged-1. *Cancer Cell.* 23:171–185. http://dx.doi.org/10.1016/j.ccr.2012.12.021

Metcalfe, C., P. Cresswell, L. Ciaccia, B. Thomas, and A.N. Barclay. 2011. Labile disulfide bonds are common at the leucocyte cell surface. *Open Biol.* 1:110010. http://dx.doi.org/10.1098/rsob.110010

Moss, M.L., M. Bomar, Q. Liu, H. Sage, P. Dempsey, P.M. Lenhart, P.A. Gillispie, A. Stoeck, D. Wildeboer, J.W. Bartsch, et al. 2007. The ADAM10 prodomain is a specific inhibitor of ADAM10 proteolytic activity and inhibits cellular shedding events. *J. Biol. Chem.* 282:35712–35721. http://dx.doi.org/10.1074/jbc.M703231200

Murphy, G. 2008. The ADAMs: signalling scissors in the tumour microenvironment. *Nat. Rev. Cancer.* 8:929–941. http://dx.doi.org/10.1038/nrc2459

Pruessmeyer, J., and A. Ludwig. 2009. The good, the bad and the ugly substrates for ADAM10 and ADAM17 in brain pathology, inflammation and cancer. *Semin. Cell Dev. Biol.* 20:167–174. http://dx.doi.org/10.1016/j.semcdb.2008.09.005

Raha, D., T.R. Wilson, J. Peng, D. Peterson, P. Yue, M. Evangelista, C. Wilson, M. Merchant, and J. Settleman. 2014. The cancer stem cell marker aldehyde dehydrogenase is required to maintain a drug-tolerant tumor cell subpopulation. *Cancer Res.* 74:3579–3590. http://dx.doi.org/10.1158/0008-5472.CAN-13-3456

Ranganathan, P., K.L. Weaver, and A.J. Capobianco. 2011. Notch signalling in solid tumours: a little bit of everything but not all the time. *Nat. Rev. Cancer.* 11:338–351. http://dx.doi.org/10.1038/nrc3035

Reiss, K., T. Maretzky, A. Ludwig, T. Tousseyn, B. de Strooper, D. Hartmann, and P. Saftig. 2005. ADAM10 cleavage of N-cadherin and regulation of cell–cell adhesion and β-catenin nuclear signalling. *EMBO J.* 24:742–752. http://dx.doi.org/10.1038/sj.emboj.7600548

Roca, C., and R.H. Adams. 2007. Regulation of vascular morphogenesis by Notch signaling. *Genes Dev.* 21:2511–2524. http://dx.doi.org/10.1101/gad.1589207

Sadeqzadeh, E., C.E. de Bock, X.D. Zhang, K.L. Shipman, N.M. Scott, C. Song, T. Yeadon, C.S. Oliveira, B. Jin, P. Hersey, et al. 2011. Dual processing of FAT1 cadherin protein by human melanoma cells generates distinct protein products. *J. Biol. Chem.* 286:28181–28191. http://dx.doi.org/10.1074/jbc.M111.234419

Saftig, P., and K. Reiss. 2011. The "A Disintegrin And Metalloproteases" ADAM10 and ADAM17: novel drug targets with therapeutic potential? *Eur. J. Cell Biol.* 90:527–535. http://dx.doi.org/10.1016/j.ejcb.2010.11.005

Sahin, U., G. Weskamp, K. Kelly, H.M. Zhou, S. Higashiyama, J. Peschon, D. Hartmann, P. Saftig, and C.P. Blobel. 2004. Distinct roles for ADAM10 and ADAM17 in ectodomain shedding of six EGFR ligands. *J. Cell Biol.* 164:769–779. http://dx.doi.org/10.1083/jcb.200307137

Smith, K.M., A. Gaultier, H. Cousin, D. Alfandari, J.M. White, and D.W. DeSimone. 2002. The cysteine-rich domain regulates ADAM protease function in vivo. *J. Cell Biol.* 159:893–902. http://dx.doi.org/10.1083/jcb.200206023

Spencer, J.D., N.C. Gibbons, M. Böhm, and K.U. Schallreuter. 2008. The Ca^{2+}-binding capacity of epidermal furin is disrupted by H_2O_2-mediated oxidation in vitiligo. *Endocrinology.* 149:1638–1645. http://dx.doi.org/10.1210/en.2007-1317

Suh, J., S.H. Choi, D.M. Romano, M.A. Gannon, A.N. Lesinski, D.Y. Kim, and R.E. Tanzi. 2013. ADAM10 missense mutations potentiate β-amyloid accumulation by impairing prodomain chaperone function. *Neuron.* 80:385–401. http://dx.doi.org/10.1016/j.neuron.2013.08.035

Takeda, S., T. Igarashi, H. Mori, and S. Araki. 2006. Crystal structures of VAP1 reveal ADAMs' MDC domain architecture and its unique C-shaped scaffold. *EMBO J.* 25:2388–2396. http://dx.doi.org/10.1038/sj.emboj.7601131

Taniguchi, K., L.W. Wu, S.I. Grivennikov, P.R. de Jong, I. Lian, F.X. Yu, K. Wang, S.B. Ho, B.S. Boland, J.T. Chang, et al. 2015. A gp130-Src-YAP module links inflammation to epithelial regeneration. *Nature.* 519:57–62. http://dx.doi.org/10.1038/nature14228

Tebbutt, N.C., A.S. Giraud, M. Inglese, B. Jenkins, P. Waring, F.J. Clay, S. Malki, B.M. Alderman, D. Grail, F. Hollande, et al. 2002. Reciprocal regulation of gastrointestinal homeostasis by SHP2 and STAT-mediated trefoil gene activation in gp130 mutant mice. *Nat. Med.* 8:1089–1097. http://dx.doi.org/10.1038/nm763

Thiem, S., T.P. Pierce, M. Palmieri, T.L. Putoczki, M. Buchert, A. Preaudet, R.O. Farid, C. Love, B. Catimel, Z. Lei, et al. 2013. mTORC1 inhibition restricts inflammation-associated gastrointestinal tumorigenesis in mice. *J. Clin. Invest.* 123:767–781. http://dx.doi.org/10.1172/JCI65086

Tsai, Y.-H., K.L. VanDussen, E.T. Sawey, A.W. Wade, C. Kasper, S. Rakshit, R.G. Bhatt, A. Stoeck, I. Maillard, H.C. Crawford, et al. 2014. ADAM10 regulates Notch function in intestinal stem cells of mice. *Gastroenterology.* 147:822–834.e13. http://dx.doi.org/10.1053/j.gastro.2014.07.003

Wang, B., T. Mysliwiec, S.M. Feller, B. Knudsen, H. Hanafusa, and G.D. Kruh. 1996. Proline-rich sequences mediate the interaction of the Arg protein tyrosine kinase with Crk. *Oncogene.* 13:1379–1385.

Wang, Y., A.H. Herrera, Y. Li, K.K. Belani, and B. Walcheck. 2009. Regulation of mature ADAM17 by redox agents for L-selectin shedding. *J. Immunol.* 182:2449–2457. http://dx.doi.org/10.4049/jimmunol.0802770

Willems, S.H., C.J. Tape, P.L. Stanley, N.A. Taylor, I.G. Mills, D.E. Neal, J. McCafferty, and G. Murphy. 2010. Thiol isomerases negatively regulate the cellular shedding activity of ADAM17. *Biochem. J.* 428:439–450. http://dx.doi.org/10.1042/BJ20100179

Woo, H.A., S.H. Yim, D.H. Shin, D. Kang, D.Y. Yu, and S.G. Rhee. 2010. Inactivation of peroxiredoxin I by phosphorylation allows localized H_2O_2 accumulation for cell signaling. *Cell.* 140:517–528. http://dx.doi.org/10.1016/j.cell.2010.01.009

Zamboni, W.C., C.F. Stewart, P.J. Cheshire, L.B. Richmond, S.K. Hanna, X. Luo, C. Poquette, J.P. McGovren, J.A. Houghton, and P.J. Houghton. 1998. Studies of the efficacy and pharmacology of irinotecan against human colon tumor xenograft models. *Clin. Cancer Res.* 4:743–753.